

Meta Flow Maps enable scalable reward alignment

Peter Potapchik^{*1,2}, Adhi Saravanan^{*1}, Abbas Mammadov¹, Alvaro Prat¹,
Michael S. Albergo^{†2,3}, Yee Whye Teh^{†1}

¹University of Oxford, ²Harvard University, ³Kempner Institute

Abstract. Controlling generative models is computationally expensive. This is because optimal alignment with a reward function—whether via inference-time steering or fine-tuning—requires estimating the value function. This task demands access to the conditional posterior $p_{1|t}(x_1|x_t)$, the distribution of clean data x_1 consistent with an intermediate state x_t , a requirement that typically compels methods to resort to costly trajectory simulations. To address this bottleneck, we introduce **Meta Flow Maps (MFMs)**, a framework extending consistency models and flow maps into the stochastic regime. MFMs are trained to perform **stochastic one-step posterior sampling**, generating arbitrarily many i.i.d. draws of clean data x_1 from any intermediate state. Crucially, these samples provide a differentiable reparametrization that unlocks efficient value function estimation. We leverage this capability to solve bottlenecks in both paradigms: enabling **inference-time steering without inner rollouts**, and facilitating **unbiased, off-policy fine-tuning** to general rewards. Empirically, our single-particle steered-MFM sampler outperforms a Best-of-1000 baseline on ImageNet across multiple rewards at a fraction of the compute.



Figure 1 Samples from a Meta Flow Map (MFM) trained on ImageNet (256 × 256). (Left) 4-step samples from a base MFM. (Right) Inference-time steering with MFMs and HPSv2 using the prompts shown. The base MFM generates images using **only class labels** and so **all** prompt alignment comes from the MFM steering with HPSv2.

1 Introduction

Many of the most powerful generative models today are transport-based, realizing generation through a time-evolving process, as in diffusion models, flow matching, and stochastic interpolants (Song et al., 2020; Ho et al., 2020; Lipman et al., 2022; Albergo et al., 2022). A growing frontier in this space is adapting these models to align

*Equal contribution. †Senior authors.

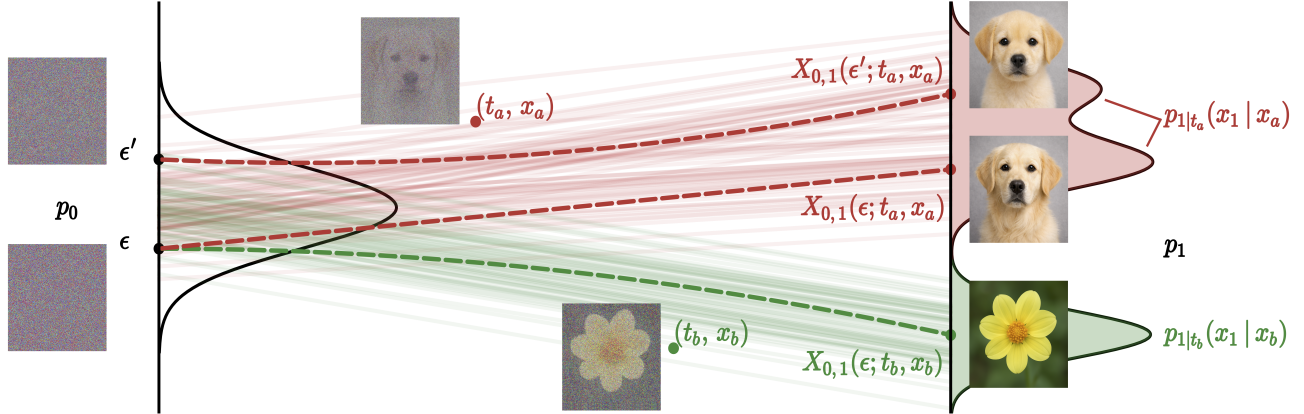


Figure 2 An MFM X conditions on an intermediate time-state pair (t, x) (visualized as noisy images) along the stochastic interpolant and learns a shared conditional flow $X_{s,u}(\cdot; t, x)$ that maps base noise $\epsilon \sim p_0$ to endpoint samples $x_1 \sim p_{1|t}(\cdot|x)$ (visualized as clean images) via $X_{0,1}(\epsilon; t, x)$. For a given (t, x) pair, varying the initial noise $\epsilon' \sim p_0$ yields multiple samples from the same posterior $p_{1|t}(\cdot|x)$. Conversely, for the same initial noise ϵ , conditioning on two different time-state pairs (t_a, x_a) and (t_b, x_b) yields one sample from each of two different posteriors $p_{1|t_a}(\cdot|x_a)$ and $p_{1|t_b}(\cdot|x_b)$.

with a reward function. In many applications, we are not satisfied with unconditional samples; instead, we want to *control* model trajectories so that samples exhibit desirable properties (Bansal et al., 2023; Kim et al., 2023; Ma et al., 2025).

Formally, this task can be phrased as sampling from a modified target, the *reward-tilted* distribution:

$$p_{\text{reward}}(x) \propto p_{\text{model}}(x) e^{r(x)}, \quad (1)$$

where $p_{\text{model}}(x)$ is the output distribution of the original pretrained generative model, and $r(x)$ is a general reward function. This formulation encapsulates settings such as classifier guidance, where $r(x) = \log p(c|x)$ targets a class c (Dhariwal et al., 2021), inverse problems, where $r(x) = \log p(y_{\text{obs}}|x)$ (Chung et al., 2024), or black-box rewards (e.g., r measures aesthetics or prompt alignment). In all cases, the central algorithmic challenge is to modify the sampling dynamics so that terminal samples are distributed according to p_{reward} .

Two related paradigms for achieving such control are *inference-time steering* and *fine-tuning*. Inference-time steering keeps the pretrained model fixed and modifies the sampling process directly—traditionally at the cost of substantially more expensive generation—in order to target p_{reward} . Fine-tuning, conversely, updates the generative network’s parameters to permanently target p_{reward} (Clark et al., 2024; Domingo-Enrich et al., 2025; Potapchik et al., 2025). While effective for a single fixed objective, repeating this computationally intensive process for every new downstream reward is often intractable.

Despite these practical distinctions, the two paradigms share a unified theoretical solution. In both cases, the optimally controlled drift targeting p_{reward} is identical, and can be expressed in terms of the value function which, for a stochastic process $(X_t)_{t \in [0,1]}$, is defined as

$$V_t(x) := \log \mathbb{E}[e^{r(X_1)} | X_t = x]. \quad (2)$$

This function measures the expected future reward conditioned on the current state x at time t , where the expectation is taken over the *conditional posterior* $p_{1|t}(\cdot|x)$ —the distribution of clean endpoints X_1 consistent with $X_t = x$. Crucially, the gradient $\nabla V_t(x)$ determines the optimal drift correction required to direct trajectories toward high-reward states (Dai Pra, 1991). This correction serves as the target for both strategies: it can be applied transiently during inference-time steering or distilled permanently into model weights during fine-tuning. Thus, both paradigms are mathematically unified by the shared bottleneck of estimating $\nabla V_t(x)$.

Estimating this gradient generally necessitates samples from the conditional posterior $p_{1|t}(\cdot|x)$, creating a fundamental computational dilemma. Heuristic approximations, such as replacing the posterior with a point mass or a Gaussian centred at the posterior mean (Song et al., 2023a; Chung et al., 2024), are efficient but biased, often failing in multimodal settings. Conversely, Monte Carlo estimation requires drawing exact samples by

integrating long ODE or SDE trajectories (Holderrieth et al., 2025; Jain et al., 2025). This reliance on repeated trajectory integration makes steering prohibitively slow and fine-tuning for every downstream reward impractical. To eliminate this bottleneck, we ask whether the computational burden can be amortized during the training of the base model by compressing these expensive rollouts into efficient, few-step maps—thereby making it feasible to efficiently steer or fine-tune on any new reward.

A natural strategy is to learn a new class of few-step maps, paralleling the development of consistency models and flow maps (Song et al., 2023c; Frans et al., 2025; Geng et al., 2025a; Boffi et al., 2025). Flow maps distill the probability flow ODE of $(X_t)_{t \in [0,1]}$ into an efficient map that predicts the trajectory endpoint x_1 from an intermediate state x . However, as *deterministic* maps of x , they are inherently incapable of representing the diversity of the conditional posterior $p_{1|t}(\cdot|x)$ since they collapse the output to a single point. We instead seek *stochastic* maps that still efficiently compress generative rollouts, but also explicitly preserve the *full* posterior distribution.

We refer to this new class of operators as *Stochastic Flow Maps*. Concretely, we define a stochastic flow map as a transformation that maps an exogenous noise source ϵ and an intermediate state x directly to a sample $x_1 \sim p_{1|t}(\cdot|x)$. By varying this noise input, the map can generate arbitrarily many i.i.d. draws from the posterior in a single step. The motivation for such maps is that these one-shot posterior samples provide a *differentiable reparametrization* of the posterior, enabling asymptotically exact estimation of the value function and its gradient. This raises the natural question: how can we efficiently train such stochastic flow maps?

To address this, we introduce **Meta Flow Maps (MFMs)**. We exploit that for any intermediate state x at time t , there exists a probability flow ODE transporting a simple noise distribution to the conditional posterior $p_{1|t}(\cdot|x)$. Since each ODE has a corresponding flow map compressing its trajectory rollouts, we reduce learning a stochastic flow map to learning this infinite collection of posterior-targeting flow maps simultaneously. MFMs achieve this by training a single amortized model that acts as a “meta” flow map over this infinite family.

Empirically, we demonstrate that MFMs train efficiently at scale and can be applied across diverse reward settings. Our results show competitive sample quality and improved controllability with marked reductions in computation for steering and fine-tuning.

Core Contributions:

- We introduce **Meta Flow Maps (MFMs)**, stochastic extensions of consistency models and flow maps that generate **arbitrarily many one-step** samples of clean data x_1 conditioned on any noisy state x_t .
- Unlike standard few-step models, MFMs capture the **full conditional posterior** $p_{1|t}(\cdot|x_t)$.
- We leverage these differentiable samples for efficient, asymptotically exact **inference-time steering** via Monte Carlo estimators of the value function and its gradient.
- We show that MFMs enable efficient **off-policy fine-tuning** to general rewards using unbiased objectives.

2 Dynamical Measure Transport

Before developing our framework, we briefly review the transport viewpoint that underpins our approach. We first recall ODE-based transport and its standard flow matching training objective, then summarize one and few-step flow map models that compress ODE integration into efficient maps.

2.1 Dynamical Transport via ODEs

ODE Transport. A central objective in modern generative modelling is to learn a transport that transforms samples from a reference distribution $x_0 \sim p_0$ into a data distribution $x_1 \sim p_1$, inferred from existing data samples $\{x_1^{(i)}\}_{i=1}^N$. Rather than modelling p_1 directly, one constructs a dynamical system that continuously evolves particles from p_0 to p_1 under a time-dependent drift $b_t : \mathbb{R}^d \rightarrow \mathbb{R}^d$. In the deterministic setting, the sample trajectories $(x_t)_{t \in [0,1]}$ evolve according to an ordinary differential equation (ODE)

$$\dot{x}_t = b_t(x_t), \quad x_0 \sim p_0. \quad (3)$$

Training. The goal now is to choose a drift b_t such that the endpoint of this ODE is distributed according to p_1 , that is $x_1 \sim p_1$. To achieve this, flow matching and stochastic interpolants (Albergo et al., 2022; Lipman et al., 2022; Liu et al., 2022) define a continuous-time stochastic process $(I_t)_{t \in [0,1]}$ that interpolates between samples from the prior $I_0 \sim p_0$ and the data $I_1 \sim p_1$ via

$$I_t = \alpha_t I_0 + \beta_t I_1, \quad (4)$$

where α_t, β_t are time-dependent coefficients satisfying $\alpha_0 = \beta_1 = 1$ and $\alpha_1 = \beta_0 = 0$. The density p_t of I_t defines a continuous family of intermediate distributions bridging p_0 and p_1 . One valid drift in (3) that generates this marginal family $(p_t)_{t \in [0,1]}$ (i.e., such that the density of x_t is p_t) is given by the conditional expectation

$$b_t(x) = \mathbb{E}[\dot{I}_t | I_t = x] = \dot{\alpha}_t \mathbb{E}[I_0 | I_t = x] + \dot{\beta}_t \mathbb{E}[I_1 | I_t = x], \quad (5)$$

where $\dot{I}_t = \dot{\alpha}_t I_0 + \dot{\beta}_t I_1$ is the time derivative of the interpolant. In particular, this drift ensures the terminal marginal constraint $x_1 \sim p_1$. In practice, b_t is parameterized by a neural network \hat{b}_t and learned by minimizing a mean-squared regression loss:

$$b_t = \arg \min_{\hat{b}_t} \int_0^1 \mathbb{E} \left\| \hat{b}_t(I_t) - \dot{I}_t \right\|^2 dt. \quad (6)$$

2.2 One and Few-Step Sampling

Sampling trajectories by numerically integrating the ODE in (3) typically requires many neural network evaluations, making inference expensive. This has motivated a class of methods including consistency models (Song et al., 2023c,b) and flow maps (Kim et al., 2024a; Frans et al., 2024; Boffi et al., 2024, 2025; Sabour et al., 2025) that aim to *compress* this integration into one or a small number of steps.

At a high level, these methods learn a map that directly predicts the state of the ODE trajectory (3) at time u from its state at time s , without explicitly simulating the infinitesimal dynamics. We formalize this via a *flow map*

$$X_{s,u} : \mathbb{R}^d \rightarrow \mathbb{R}^d, \quad X_{s,u}(x_s) = x_u, \quad \forall s, u \in [0, 1], \quad (7)$$

which learns the exact ODE solution operator between times s and u for trajectories $(x_t)_{t \in [0,1]}$. For training, it is convenient to parametrize the flow map in residual form

$$X_{s,u}(x) = x + (u - s) v_{s,u}(x), \quad (8)$$

where $v_{s,u}(x)$ represents the *average velocity* of the trajectory between times s and u . For $X_{s,u}$ to be consistent with the underlying ODE, the average drift must recover the instantaneous drift in the infinitesimal limit. This is captured by the tangent condition (Kim et al., 2024b),

$$\lim_{s \rightarrow u} \partial_u X_{s,u}(x) = v_{u,u}(x) = b_u(x). \quad (9)$$

In practice, we learn a neural parameterization $\hat{v}_{s,u}$, along with its induced flow map $\hat{X}_{s,u}$. A natural way to enforce the tangent condition along the diagonal $s = u$ is via a flow matching objective as in (6):

$$\mathcal{L}_b(\hat{v}) = \int_0^1 \mathbb{E} \left\| \hat{v}_{u,u}(I_u) - \dot{I}_u \right\|^2 du, \quad (10)$$

where (I_u, \dot{I}_u) are drawn from the interpolant process (4). While the diagonal loss enforces the correct instantaneous drift by matching $\hat{v}_{u,u}$ to b_u , it does not constrain the behaviour of $\hat{v}_{s,u}$ for $s \neq u$. To propagate this local correctness into a valid global trajectory, existing methods introduce an additional *consistency objective*. In particular, a valid flow map must ensure that $\hat{v}_{s,u}$ correctly represents the average drift, which is equivalent to enforcing any of the following consistency rules (Boffi et al., 2024, 2025):

$$\partial_u X_{s,u}(x) = v_{u,u}(X_{s,u}(x)), \quad \partial_s X_{s,u}(x) + v_{s,s}(x) \cdot \nabla X_{s,u}(x) = 0, \quad X_{w,u}(X_{s,w}(x)) = X_{s,u}(x). \quad (11)$$

A consistency objective must therefore ensure that one (and hence all) of the above rules is satisfied. Many flow map losses in the literature, including Consistency Trajectory, Mean Flow, and Shortcut (Kim et al., 2024b; Geng et al., 2025a; Frans et al., 2025), can be interpreted this way. For clarity, we focus on the following three losses, which directly penalize the residual violations of the above rules for all $s, u, w \in [0, 1]$ and $x \in \mathbb{R}^d$:

$$\left\| \partial_u \hat{X}_{s,u}(x) - \hat{v}_{u,u}(\hat{X}_{s,u}(x)) \right\|^2, \quad \left\| \partial_s \hat{X}_{s,u}(x) + \hat{v}_{s,s}(x) \cdot \nabla \hat{X}_{s,u}(x) \right\|^2, \quad \left\| \hat{X}_{w,u}(\hat{X}_{s,w}(x)) - \hat{X}_{s,u}(x) \right\|^2. \quad (12)$$

3 Reward Alignment

We now address aligning generative models with a reward function, a task that motivates our development of Meta Flow Maps. As discussed in Section 1, both inference-time steering and fine-tuning share a unified theoretical objective: sampling from the *reward-tilted distribution* p_{reward} defined in (1). Assuming our trained model b_t perfectly targets the data distribution, $p_{\text{model}} = p_1$, we can rewrite the target as

$$p_{\text{reward}}(x) \propto p_1(x) e^{r(x)}, \quad (13)$$

for some scalar reward function $r : \mathbb{R}^d \rightarrow \mathbb{R}$. As highlighted in Section 1, this formulation captures a diverse range of settings, including class-conditional generation, inverse problems, and black-box rewards. We begin by reviewing Doob’s h -transform, which characterizes the *optimal controlled* dynamics for targeting p_{reward} . We then outline the computational limitations of existing generative models for efficient control, motivating the need for a new class of operators.

3.1 Controlling Dynamics via Doob’s h -Transform

Recall that the drift b_t in (3) was chosen such that the ODE marginals match the interpolant’s: $\text{Law}(x_t) = \text{Law}(I_t) = p_t$. A standard approach to obtain stochastic dynamics with these same marginals is to introduce diffusion while compensating in the drift (Song et al., 2020; Albergo et al., 2023a), yielding the following SDE:

$$dX_t = \left[b_t(X_t) + \frac{\sigma_t^2}{2} \nabla \log p_t(X_t) \right] dt + \sigma_t dB_t, \quad X_0 \sim p_0, \quad (14)$$

where the diffusion coefficient is $\frac{\sigma_t^2}{2} = \frac{\dot{\beta}_t}{\beta_t} \alpha_t^2 - \dot{\alpha}_t \alpha_t$. While any diffusion schedule σ_t in this formulation yields the correct marginals $\text{Law}(X_t) = p_t$, the SDE X_t and the interpolant I_t generally possess different transition kernels. We employ this specific schedule because it ensures that the conditional endpoints laws are identical; that is, the distribution of X_1 conditioned on $X_t = x$ matches that of I_1 conditioned on $I_t = x$ (we verify this in Appendix C). Consequently, we let $p_{1|t}(\cdot|x)$ denote the density of this shared *conditional posterior distribution*:

$$p_{1|t}(\cdot|x) = \text{Law}(X_1 | X_t = x) = \text{Law}(I_1 | I_t = x). \quad (15)$$

For the SDE (14), we recall the *value function* $V_t(x)$ defined in (2):

$$V_t(x) = \log \mathbb{E}[e^{r(X_1)} | X_t = x] = \log \mathbb{E}[e^{r(I_1)} | I_t = x], \quad (16)$$

where the second equality holds precisely because the SDE and the interpolant share identical conditional endpoint laws. Doob’s h -transform (Dai Pra, 1991; Denker et al., 2025) tilts the path measure by the terminal reward $e^{r(X_1)}$ by adding the diffusion-scaled gradient of the value function to the drift, yielding the optimally controlled SDE:

$$dX_t^* = \left[b_t(X_t^*) + \frac{\sigma_t^2}{2} \nabla \log p_t(X_t^*) + \sigma_t^2 \nabla V_t(X_t^*) \right] dt + \sigma_t dB_t, \quad X_0^* \sim p_0. \quad (17)$$

Crucially, the score term in (17) corresponds to the uncontrolled process and is therefore already available; when p_0 is Gaussian, the score $\nabla \log p_t$ is simply a linear reparameterization of b_t . This leaves ∇V_t as the only missing component. Under optimal control, the marginal density p_t^* of X_t^* satisfies

$$p_t^*(x) \propto p_t(x) e^{V_t(x)}, \quad (18)$$

ensuring the terminal marginal is exactly $p_1^* = p_{\text{reward}}$. We can also define the corresponding probability flow ODE, whose trajectories satisfy $\text{Law}(x_t^*) = \text{Law}(X_t^*) = p_t^*$, by subtracting half the diffusion-scaled score from the drift:

$$\dot{x}_t^* = \underbrace{b_t(x_t^*)}_{b_t^*(x_t^*)} + \frac{\sigma_t^2}{2} \nabla V_t(x_t^*), \quad x_0^* \sim p_0. \quad (19)$$

The optimal drift b_t^* serves as the target for both control paradigms: it can be estimated to steer trajectories during inference, or distilled permanently into a student model during fine-tuning. Since b_t is readily available from the pretrained model, the central algorithmic challenge is efficiently estimating the value function gradient $\nabla V_t(x)$.

3.2 Estimators of ∇V_t

We present two consistent Monte Carlo estimators for $\nabla V_t(x)$. The limitations of existing generative models to tractably implement them will motivate the development of Meta Flow Maps.

Adapted from Tilt Matching (Potapchik et al., 2025), this estimator requires only reward function evaluations $r(x)$ and i.i.d. samples from the posterior $p_{1|t}(\cdot|x)$.

Gradient-Free Estimator (MFM-GF). A consistent Monte Carlo estimator of $\nabla V_t(x)$ is

$$\frac{\sigma_t^2}{2} \widehat{\nabla V_t(x)} = \left(\dot{\beta}_t - \frac{\dot{\alpha}_t}{\alpha_t} \beta_t \right) \frac{\sum_{i=1}^N x_1^{(i)} \exp(r(x_1^{(i)}))}{\sum_{i=1}^N \exp(r(x_1^{(i)}))} + \frac{\dot{\alpha}_t}{\alpha_t} x - b_t(x), \quad x_1^{(i)} \stackrel{\text{iid}}{\sim} p_{1|t}(\cdot|x). \quad (20)$$

If the reward function is differentiable, we can leverage the reparametrization trick (Kingma et al., 2022). Assume posterior samples can be generated via a differentiable map $\hat{x}_1 = \Phi(\epsilon; t, x)$, so that $\hat{x}_1 \sim p_{1|t}(\cdot|x)$ where $\epsilon \sim q$ for some base noise distribution q . Then we can express the gradient as:

$$\nabla V_t(x) = \nabla \log \mathbb{E}_{\epsilon \sim q} \left[\exp(r(\Phi(\epsilon; t, x))) \right]. \quad (21)$$

From this representation, we derive the following gradient-based estimator of the value function's gradient.

Gradient-Based Estimator (MFM-G). A consistent Monte Carlo estimator of $\nabla V_t(x)$ is

$$\widehat{\nabla V_t(x)} = \nabla_x \log \left(\frac{1}{N} \sum_{i=1}^N \exp(r(\Phi(\epsilon^{(i)}; t, x))) \right), \quad \epsilon^{(i)} \stackrel{\text{iid}}{\sim} q. \quad (22)$$

For steering, estimating ∇V_t must be done online at every step. For fine-tuning, this gradient defines the regression target. As this estimation must occur at every step, the viability of our approach hinges critically on our ability to sample from the conditional posterior efficiently, and for MFM-G in a differentiable manner.

3.3 Limitations of Existing Posterior Samplers

As we now discuss, obtaining posterior samples from $p_{1|t}(\cdot|x)$ to Monte Carlo estimate the gradient of the value function ∇V_t remains a major bottleneck. Existing approaches typically rely on expensive trajectory unrolling, while standard acceleration techniques like consistency models and flow maps are structurally ill-suited for conditional sampling.

Inner rollouts of SDEs. A direct way to obtain posterior samples is via “inner rollouts”, where one simulates the SDE (14) forward from time t to 1, starting at x (Elata et al., 2023; Li et al., 2025; Zhang et al., 2025; Jain et al., 2025). By repeating this process with independent noise, one yields a batch of samples from $p_{1|t}(\cdot|x)$. However, this approach is prohibitively costly, as it nests a full inner simulation within every step of the outer steering trajectory or every iteration of the fine-tuning loop.

Inner rollouts of ODEs. In principle, SDE simulation can be replaced with ODE sampling. Theoretically, for any context (t, x) , there exists an ODE that transports the prior p_0 to the conditional posterior $p_{1|t}(\cdot|x)$. The drift $\bar{b}_s(\cdot; t, x)$ for this flow can be defined as the solution to the flow matching problem in (6), targeting the conditional posterior $p_{1|t}(\cdot|x)$ rather than the marginal data distribution p_1 :

$$\bar{b}_s(\bar{x}; t, x) = \mathbb{E} [\dot{\alpha}_s \bar{I}_0 + \dot{\beta}_s \bar{I}_1 | \bar{I}_s = \bar{x}], \quad \bar{I}_s = \alpha_s \bar{I}_0 + \beta_s \bar{I}_1, \quad \bar{I}_0 \sim p_0, \bar{I}_1 \sim p_{1|t}(\cdot|x). \quad (23)$$

Consequently, the probability flow associated with $\bar{b}_s(\cdot; t, x)$ satisfies:

$$\frac{d}{ds} \bar{x}_s = \bar{b}_s(\bar{x}_s; t, x), \quad \bar{x}_0 \sim p_0 \implies \text{Law}(\bar{x}_1) = p_{1|t}(\cdot|x). \quad (24)$$

Here, we use the bar notation (\bar{x}_s, \bar{b}_s) to distinguish the state and velocity of this *conditional* auxiliary process from the unconditional trajectory (x_t, b_t) in (3). For brevity, the dependence of \bar{x}_s on (t, x) is suppressed.

Although \bar{b}_s is well defined in theory, it is generally intractable without retraining. However, when the prior p_0 is Gaussian, GLASS flows (Holderrieth et al., 2025) demonstrate that \bar{b}_s can be derived analytically by reparameterizing the drift b_t :

$$\bar{b}_s(\bar{x}_s; t, x) = w_1 \bar{x}_s + w_2 b_{t^*}(S(\bar{x}_s, x)) + w_3 x, \quad (25)$$

where w_1, w_2, w_3 are scalar coefficients, t^* is a reparametrized time, and S is a linear sufficient statistic. We provide explicit expressions for these terms in Appendix D. While this reparametrization makes \bar{b}_s accessible, generating posterior samples from $p_{1|t}(\cdot|x)$ by unrolling ODE trajectories remains computationally expensive. It requires drawing a separate initial condition $\bar{x}_0 \sim p_0$ for every element in the Monte Carlo batch and integrating (24).

Furthermore, efficient estimators of $\nabla V_t(x)$, such as (22), also require that the posterior samples $x_1 \sim p_{1|t}(\cdot|x)$ are differentiable with respect to x via the reparametrization Φ . While it is theoretically possible to differentiate through the ODE or SDE solvers used in exact rollouts, this incurs a prohibitive memory and computational cost, making it impractical for iterative steering or fine-tuning. Consequently, this has often forced reliance on coarse approximations.

Insufficiency of flow maps. Finally, we remark that standard flow maps address a fundamentally different transport problem than what is required for posterior sampling. A flow map $X_{s,u}$ is trained to satisfy the *marginal* transport constraint:

$$X_{s,u} \# p_s = p_u, \quad \forall s, u \in [0, 1]. \quad (26)$$

Because the map $x \mapsto X_{t,1}(x)$ is a deterministic function of x , it is structurally incapable of representing the full conditional posterior $p_{1|t}(\cdot|x)$, which generally admits a distribution of valid endpoints for any fixed intermediate state x at time t .

This leaves us with a fundamental dilemma. Exact sampling methods, such as SDE or ODE rollouts, can capture the diversity of the posterior but are prohibitively slow due to the need for iterative integration. Conversely, accelerated methods like consistency models and flow maps are efficient but, due to their deterministic nature, cannot capture the stochasticity required for posterior sampling.

4 Meta Flow Maps

To solve this computational bottleneck, we require a new type of model that bridges this gap: an operator that retains the one-step efficiency of flow maps but introduces the stochasticity necessary to cover the full support of every posterior. We first introduce the formalism for such operators with Stochastic Flow Maps—generalized maps for stochastic one-step sampling. We then introduce Meta Flow Maps (MFMs), a practical amortized framework for training them.

4.1 Stochastic Flow Maps

Standard flow maps are deterministic operators designed to transport a source distribution to a *single* target distribution. To capture entire families of target distributions, we must extend this framework to the stochastic regime.

Definition (Stochastic Flow Map). Let \mathcal{C} be an index set of contexts. For each context $c \in \mathcal{C}$, let p_c be a target distribution on \mathbb{R}^d . A Stochastic Flow Map is a parametric function $\Phi(\epsilon; c) : \mathbb{R}^d \times \mathcal{C} \rightarrow \mathbb{R}^d$ that maps exogenous noise $\epsilon \sim q$ directly to the target p_c . Specifically, it satisfies the *conditional* transport constraint:

$$\Phi(\cdot; c) \# q = p_c, \quad \forall c \in \mathcal{C}. \quad (27)$$

The inclusion of ϵ renders Φ stochastic with respect to c . This allows Φ to generate arbitrarily many distinct samples for a fixed context, enabling it to cover the full support of each p_c . However, this formulation leaves open the core problem: how to train such a map to target the family of conditional posteriors we are interested in.

Problem. How can we train efficient stochastic flow maps that sample from the entire family $p_{1|t}(\cdot|x)$?

4.2 Meta Flow Map Framework

Target family. For our goals with reward alignment, we desire a stochastic flow map that targets the family of conditional posteriors. Therefore, we will identify the context c with the time-state pair (t, x) from the generative process, and set $\mathcal{C} = [0, 1] \times \mathbb{R}^d$. Our target family is the set of conditional posteriors $\mathcal{P} := \{p_{1|t}(\cdot|x)\}_{(t,x) \in [0,1] \times \mathbb{R}^d}$.

Family of conditional probability flow ODEs. We recall from Section 3.3, that for any specific context (t, x) , there exists a probability flow ODE (24) transporting p_0 to $p_{1|t}(\cdot|x)$. Each of these posterior-targeting ODEs has a dedicated flow map which is its solution operator. We define a Meta Flow Map as an amortized map for this collection.

Definition (Meta Flow Map). A Meta Flow Map (MFM) targeting the family \mathcal{P} is the parametric family of conditional flow maps $X_{s,u}(\cdot; t, x) : \mathbb{R}^d \rightarrow \mathbb{R}^d$ acting as the solution operators for the context-dependent ODEs in (24). Formally, for any trajectory $(\bar{x}_\tau)_{\tau \in [0,1]}$ governed by the specific drift $\bar{b}_\tau(\cdot; t, x)$, the map satisfies:

$$X_{s,u}(\bar{x}_s; t, x) = \bar{x}_u, \quad \forall s, u \in [0, 1]. \quad (28)$$

In particular, by setting $q = p_0$, the MFM X satisfies the definition of a stochastic flow map in (27).

Here, the context (t, x) specifies the target posterior, while s and u denote flow times of the auxiliary probability flow ODE. The qualifier ‘‘meta’’ highlights that our model does not learn only a single transport map, but rather a family of transport maps, one for each context (t, x) . As such, the context acts to ‘‘choose’’ the flow map that targets the specific posterior $p_{1|t}(\cdot|x)$. See Figures 2 and 3 for an overview.

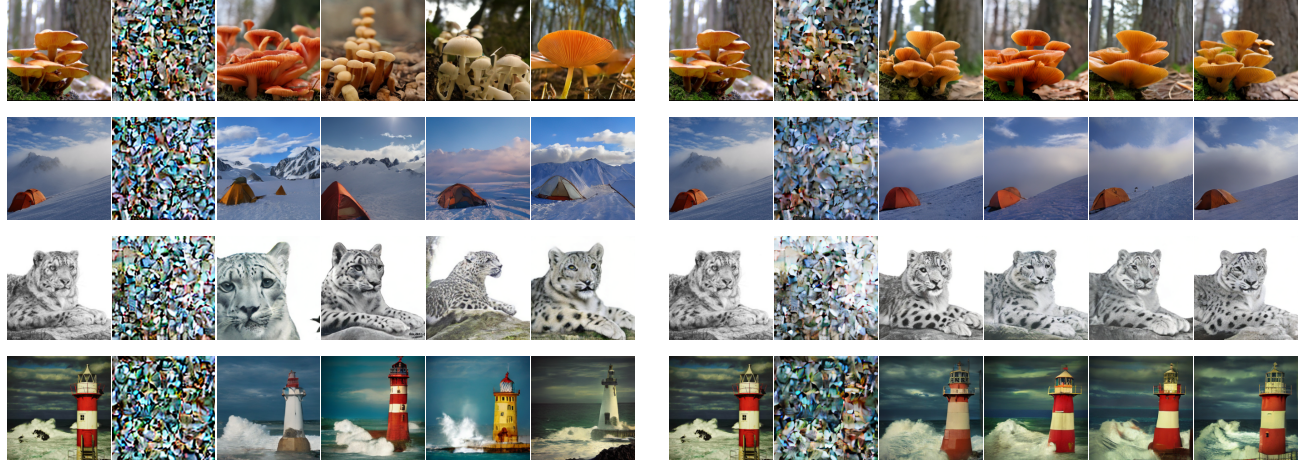
Auxiliary transport. To avoid confusion, we emphasize that the MFM’s auxiliary flow $(\bar{x}_s)_{s \in [0,1]}$ does not reproduce the conditional evolution of the generative process, whether modelled as the SDE (X_t) or the interpolant (I_t). While a generative trajectory conditioned on state x at time t is naturally constrained to intersect x , the MFM trajectories $(\bar{x}_s)_{s \in [0,1]}$ are not, implying that in general $X_{0,t}(\epsilon; t, x) \neq x$. The MFM is instead designed solely to satisfy the endpoint constraint $\bar{x}_1 \sim p_{1|t}(\cdot|x)$ starting from noise at $s = 0$. Consequently, the auxiliary trajectory \bar{x}_s need not intersect x at any point, and the intermediate states \bar{x}_s for $s < 1$ generally lack a direct interpretation. This distinction is highlighted in Figure 2, where the bold dotted trajectories clearly do not pass through the conditioning points (t_a, x_a) or (t_b, x_b) .

4.3 Training

For training, it is convenient to parametrize the MFM with a neural network in residual form,

$$\hat{X}_{s,u}(\bar{x}; t, x) = \bar{x} + (u - s)\hat{v}_{s,u}(\bar{x}; t, x), \quad (29)$$

where \hat{v} predicts the average velocity of the auxiliary trajectory. Note that for any *fixed* context pair (t, x) , the subnetwork $\hat{X}_{s,u}(\cdot; t, x)$ acts as a standard flow map targeting the specific conditional posterior $p_{1|t}(\cdot|x)$.



(a) Large noise level ($t = 0.2$), where the posterior is broad and the samples exhibit noticeable variation while remaining semantically consistent with the original image.

(b) Small noise level ($t = 0.4$), where the posterior concentrates and the conditional samples are nearly identical to each other and to the original image.

Figure 3 Conditional endpoint samples on ImageNet. In each block, the first column shows a ground-truth ImageNet image, the second column shows a corrupted version x_t at the indicated noise level, and the remaining four columns are four independent one-shot samples from the Meta Flow Map, $\hat{x}_1^{(i)} = X_{0,1}(\epsilon^{(i)}; t, x_t)$, targeting $p_{1|t}(\cdot | x_t)$, for independent $\epsilon^{(i)}$. The noise variables $\epsilon^{(i)}$ for the posterior-sample columns are coupled across the left and right sub-figures, showing how the same $\epsilon^{(i)}$ yields different endpoints as (t, x_t) changes.

Therefore, we can train it using standard flow map objectives, amortizing over all possible contexts by randomly sampling (t, x) . We employ a *diagonal loss* to anchor the instantaneous velocity field $\hat{v}_{s,s}(\cdot; t, x)$ to the theoretical velocity $\bar{b}_s(\cdot; t, x)$ of the auxiliary conditional ODE. We use an additional *consistency loss* to ensure the map $\hat{X}_{s,u}(\cdot; t, x)$ integrates this instantaneous velocity correctly over time intervals (s, u) , resulting in a valid flow map for each fixed (t, x) . We define these terms below for two distinct training scenarios: training directly from data and distillation.

4.3.1 Training from Data

When training on a dataset, we lack access to the ground-truth vector field \bar{b}_s . Instead, we construct simulation-free targets using the stochastic interpolant framework and employ a self-distillation consistency loss.

Diagonal loss $\mathcal{L}_{\text{diag}}$. Recall that \bar{b}_s is defined as the solution to a conditional flow matching problem (23). Therefore, to supervise the instantaneous velocity $\hat{v}_{s,s}$, we construct reference trajectories that connect the prior to the correct conditional posterior. We sample times $s, t \sim \text{Unif}[0, 1]$, draw a data sample $I_1 \sim p_1$, set $\bar{I}_1 = I_1$, draw independent prior samples $I_0, \bar{I}_0 \sim p_0$, and construct two coupled interpolants:

$$I_t = \alpha_t I_0 + \beta_t \bar{I}_1, \quad \bar{I}_s = \alpha_s \bar{I}_0 + \beta_s \bar{I}_1. \quad (30)$$

Conditioned on the context state $I_t = x$, the endpoint I_1 is distributed exactly according to $p_{1|t}(\cdot | x)$, implying that $\text{Law}(\bar{I}_0, \bar{I}_1 | I_t = x) = p_0 \times p_{1|t}(\cdot | x)$. Therefore, the auxiliary path \bar{I}_s traces a valid conditional trajectory from p_0 to this posterior. We treat its time derivative, $\frac{d}{ds} \bar{I}_s = \dot{\alpha}_s \bar{I}_0 + \dot{\beta}_s \bar{I}_1$, as the regression target for the diagonal loss:

$$\mathcal{L}_{\text{diag}}^{\text{data}}(\hat{v}) := \int_0^1 \int_0^1 \mathbb{E} \left\| \hat{v}_{s,s}(\bar{I}_s; t, I_t) - \frac{d}{ds} \bar{I}_s \right\|^2 ds dt. \quad (31)$$

Minimizing the diagonal loss ensures that $\hat{v}_{s,s}(\bar{x}; t, x) = \bar{b}_s(\bar{x}; t, x)$ for all $t \in [0, 1], \bar{x}, x \in \mathbb{R}^d$.

Self-distillation consistency loss $\mathcal{L}_{\text{cons}}$. We require a consistency loss to ensure $\hat{v}_{s,u}$ learns the average velocity for $s \neq u$. This is equivalent to enforcing any of the consistency rules in (11) on the map $\hat{X}_{s,u}(\cdot; t, x)$ for

every (t, x) . Therefore, one simply applies *any* standard self-consistency loss to this conditional map $\hat{X}_{s,u}(\cdot; t, x)$. Table 1 explicitly details four representative examples, though we emphasize that our framework is agnostic to this choice. Note that we rely on self-distillation, where the student \hat{v} bootstrap its own targets, effectively enforcing consistency relative to its own current predictions.

Table 1 MFM consistency objectives. We adapt the Eulerian, Lagrangian, and Semigroup losses (Boffi et al., 2025) and the Mean Flow loss (Geng et al., 2025a) to the MFM framework. We distinguish between two supervision variants: teacher-distillation, which leverages the analytical drift \bar{b}_s of a pretrained flow matching model b_t for stable supervision, and self-distillation, where the model bootstraps its own targets when training directly from data. The operator $sg(\cdot)$ signifies that we place a stop gradient on the term during optimization.

Objective	Distillation	Loss Formulation $\mathcal{L}_{\text{cons}}(\hat{v})$
Eulerian	Self	$\int_0^1 \int_0^u \mathbb{E} \left\ \hat{v}_{s,u}(I_s; t, I'_t) - sg((u-s)\partial_s \hat{v}_{s,u}(I_s; t, I'_t) + v_{s,s}(I_s; t, I'_t) \cdot \nabla \hat{X}_{s,u}(I_s; t, I'_t)) \right\ ^2 ds du$
	Teacher	$\int_0^1 \int_0^u \mathbb{E} \left\ \hat{v}_{s,u}(I_s; t, I'_t) - sg((u-s)\partial_s \hat{v}_{s,u}(I_s; t, I'_t) + \bar{b}_s(I_s; t, I'_t) \cdot \nabla \hat{X}_{s,u}(I_s; t, I'_t)) \right\ ^2 ds du$
Lagrangian	Self	$\int_0^1 \int_0^u \mathbb{E} \left\ \hat{v}_{s,u}(I_s; t, I'_t) - sg(\hat{v}_{u,u}(\hat{X}_{s,u}(I_s; t, I'_t); t, I'_t) - (u-s)\partial_u \hat{v}_{s,u}(I_s; t, I'_t)) \right\ ^2 ds du$
	Teacher	$\int_0^1 \int_0^u \mathbb{E} \left\ \hat{v}_{s,u}(I_s; t, I'_t) - sg(\bar{b}_u(\hat{X}_{s,u}(I_s; t, I'_t); t, I'_t) - (u-s)\partial_u \hat{v}_{s,u}(I_s; t, I'_t)) \right\ ^2 ds du$
Mean Flow	Self	$\int_0^1 \int_0^u \mathbb{E} \left\ \hat{v}_{s,u}(I_s; t, I'_t) - sg((u-s)\partial_s \hat{v}_{s,u}(I_s; t, I'_t) + \dot{I}_s \cdot \nabla \hat{X}_{s,u}(I_s; t, I'_t)) \right\ ^2 ds du$
Semigroup	Self	$\int_0^1 \int_0^u \int_s^u \mathbb{E} \left\ \hat{X}_{s,u}(I_s; t, I'_t) - sg(\hat{X}_{w,u}(\hat{X}_{s,w}(I_s; t, I'_t); t, I'_t)) \right\ ^2 dw ds du$

4.3.2 Training via Distillation

When a pretrained flow matching model with drift b_t is available, we can distill it directly into an MFM, provided the base distribution p_0 is Gaussian. We use the pretrained model to construct the target conditional vector fields.

Diagonal loss $\mathcal{L}_{\text{diag}}$. To supervise the instantaneous velocity $\hat{v}_{s,s}$, we substitute the simulation-free data target used in Section 4.3.1 with the ground-truth conditional drift $\bar{b}_s(\cdot; t, x)$. As discussed in Section 3.3, \bar{b}_s can be derived analytically from the unconditional teacher drift b_t via the GLASS flow reparameterization (Holderrieth et al., 2025). We regress the MFM’s diagonal directly onto this analytical target:

$$\mathcal{L}_{\text{diag}}^{\text{teach}}(\hat{v}) := \int_0^1 \int_0^1 \mathbb{E} \left\| \hat{v}_{s,s}(\bar{x}; t, x) - \bar{b}_s(\bar{x}; t, x) \right\|^2 ds dt, \quad (32)$$

where the expectation is over the distribution of the query points \bar{x} and x . These can be either constructed from data or from simulating trajectories with the teacher b_t . We provide explicit expressions for \bar{b}_s in terms of b_t in Appendix D. Crucially, since the target vector field is explicitly defined by the teacher, this objective admits a global minimum of zero.

Consistency loss $\mathcal{L}_{\text{cons}}$. We again require a consistency loss to ensure the map $\hat{X}_{s,u}$ correctly integrates the velocity field for $s \neq u$. While self-distillation is possible, we favour a *teacher-distillation* approach: since the ground-truth conditional velocity field \bar{b}_s is available analytically via GLASS, we can replace the unstable bootstrap targets in the consistency objectives with fixed targets derived directly from \bar{b}_s . For instance, in the Lagrangian objective, we replace the student’s velocity estimate $\hat{v}_{u,u}$ with the teacher’s \bar{b}_u . This provides more stable targets for training; we detail these teacher-distillation variants in Table 1.

MFM Objective. Combining the two terms, we define the total MFM training objective as:

$$\mathcal{L}_{\text{MFM}}(\hat{v}) := \mathcal{L}_{\text{diag}}(\hat{v}) + \mathcal{L}_{\text{cons}}(\hat{v}). \quad (33)$$

Here, $\mathcal{L}_{\text{diag}}$ provides diagonal supervision via data (31) or teacher-distillation (32), while $\mathcal{L}_{\text{cons}}$ enforces consistency on the conditional map $\hat{X}_{s,u}(\cdot; t, x)$ using objectives such as those in Table 1. Minimizing (33) over \hat{v} ensures that \hat{X} satisfies the definition of a stochastic flow map in (27) with base noise $q = p_0$. Consequently, the map $\hat{X}_{0,1}(\epsilon; t, x)$ generates one-shot samples directly from the conditional posterior $p_{1|t}(\cdot|x)$ for $\epsilon \sim p_0$.

4.4 Extensions to General Stochastic Processes and Contexts

While we have focused on learning stochastic flow maps for the specific family of posteriors $p_{1|t}(\cdot|x)$ arising from linear interpolants, our framework extends naturally to *arbitrary* context sets and *general* stochastic processes.

Consider a stochastic process $(X_\tau)_{\tau \in \mathcal{T}}$ (e.g., video frames or weather observations), which need not be an interpolant or defined by a flow matching process. We define a general context $c = \{(t_i, x_i)\}_{i=1}^M$ as a set of observations at various times and let $r \in \mathcal{T}$ be an arbitrary prediction time. Our objective is to learn an extended Meta Flow Map $X_{s,u}(\cdot; r, c)$ that samples from the generalized posterior by satisfying the transport:

$$X_{0,1}(\cdot; r, c) \# q = p_{r|c}(\cdot|c) := \text{Law}(X_r | X_{t_1} = x_1, \dots, X_{t_M} = x_M). \quad (34)$$

To achieve this, we define a conditional drift $\bar{b}_s(\cdot; r, c)$ to construct an auxiliary probability flow over a computational time $s \in [0, 1]$ that transports a base measure q to the generalized posterior $p_{r|c}$. The MFM is then trained as the solution operator for this family of auxiliary ODEs. See Appendix A.5 for further details.

4.5 Sampling

MFMs support several approaches to sampling from p_1 , either in one shot or as a multi-step refinement.

One-step sampler. A simple sampler draws $\epsilon \sim p_0$ and applies the one-step map at $t = 0$ for any choice of $x \in \mathbb{R}^d$:

$$\hat{x}_1 = X_{0,1}(\epsilon; 0, x). \quad (35)$$

Since I_0 is independent of I_1 , for any x we have that $p_{1|0}(\cdot|x) = p_1$. Thus a perfectly trained MFM yields $\hat{x}_1 \sim p_1$.

Algorithm 1 K -Step MFM Sampler

Require: MFM X , times $0 = t_0 < \dots < t_K = 1$.

```

1: Sample  $x_0 \sim p_0$ 
2: for  $k = 0, \dots, K - 1$  do
3:   Sample  $\epsilon^{(k)}, x_0^{(k)} \stackrel{\text{iid}}{\sim} p_0$ 
4:    $\hat{x}_1^{(k)} \leftarrow X_{0,1}(\epsilon^{(k)}; t_k, x_{t_k})$ 
5:    $x_{t_{k+1}} \leftarrow \alpha_{t_{k+1}} x_0^{(k)} + \beta_{t_{k+1}} \hat{x}_1^{(k)}$ 
6: end for
7: return  $x_1$ 

```

K -step sampler. We can sample using a K -step refinement procedure as outlined in Algorithm 1. With a well-trained MFM, each $\hat{x}_1^{(k)} \sim p_1$, so $x_{t_{k+1}}$ has marginal density $p_{t_{k+1}}$ for all k . This iterative procedure improves sample quality, as it increasingly relies on one-step maps at larger conditioning times t , which are typically easier to learn accurately. While we show the algorithm using the same Gaussian path as the original interpolant (4), by reparametrization the same K -step sampler applies to any other interpolant path $\tilde{\alpha}_t, \tilde{\beta}_t$ (see Appendix A.1). See Appendix A.4 for a discussion on the connection to γ -sampling.

5 MFMs for Reward Alignment

5.1 Inference - Time Steering

Next, we demonstrate how MFMs enable efficient inference-time steering. Our core approach is to estimate the optimal steering drift directly and to simulate the resulting steered dynamics.

As established in Section 3, the optimally steered processes (17) and (19) targeting p_{reward} are governed by drifts that combine the marginal drift b_t , the score $\nabla \log p_t$, and the gradient of the value function ∇V_t . We can extract b_t and $\nabla \log p_t$ directly from a trained MFM, but we must estimate the value function's gradient.

Extracting the unconditional drift and score. The first component, the marginal drift b_t , corresponds to the unconditional flow from p_0 to p_1 . Recall that for any $x_0 \in \mathbb{R}^d$, the conditional distribution $p_{1|0}(\cdot|x_0)$ is simply the marginal data distribution p_1 . Consequently, the flow map $X_{s,u}(\cdot; 0, x_0)$ recovers the unconditional flow governed by b_t . By the tangent condition (9), we can extract the instantaneous drift for any state $x \in \mathbb{R}^d$ using any conditioning point x_0 :

$$b_t(x) = v_{t,t}(x; 0, x_0). \quad (36)$$

If the base distribution p_0 is Gaussian, then the score function $\nabla \log p_t(x)$ required for SDE simulation is also available via a linear reparameterization of this drift b_t (Albergo et al., 2023a). Rather than explicitly forming b_t , one can also perform Euler-style updates using short flow segments (see Appendix A.2).

Estimating ∇V_t . We return to the core motivation in the construction of MFM, estimation of the gradient of the value function. We leverage the estimators, $\widehat{\nabla V_t(x)}$ from Section 3.2, which require computing expectations over the conditional posterior $p_{1|t}(\cdot|x)$. Recalling the specific diffusion schedule σ_t assumed earlier, the MFM generates direct samples from the posterior of the SDE (14) via $X_{0,1}(\epsilon; t, x)$ for $\epsilon \sim p_0$. More general SDEs can be handled via reparametrization (see Appendix A.1).

Given access to these posterior samples, we can directly implement MFM-GF (20). To implement MFM-G (22), we set $q = p_0$ and $\Phi = X_{0,1}$, giving the estimator:

$$\widehat{\nabla V_t(x)} = \nabla_x \log \left(\frac{1}{N} \sum_{i=1}^N \exp(r(X_{0,1}(\epsilon^{(i)}; t, x))) \right), \quad \epsilon^{(i)} \stackrel{\text{iid}}{\sim} p_0. \quad (37)$$

We remark that the estimators (20) and (22) are not specific to MFM; they hold for any stochastic flow map that satisfies the conditional transport constraint. We also note that similar estimators to (22) have appeared in the steering literature before. However, since prior works lacked access to efficient, differentiable samples from the true conditional posterior, they relied on heuristic approximations. For instance, Bansal et al. (2023); Yu et al. (2023); Chung et al. (2024) can be interpreted as approximating the estimator with a point mass at the denoising mean estimate. Similarly, Song et al. (2023a) explicitly acknowledges the intractability of the true posterior and approximates it as a Gaussian centered at the denoising mean. Consequently, the practical utility of these estimators has historically been constrained by the prohibitive cost of exact trajectory unrolling or the bias of these heuristic approximations. Stochastic flow maps, such as MFM, overcome this bottleneck by providing the efficient, differentiable access to $p_{1|t}(\cdot|x)$ required to deploy these estimators faithfully.

Steering via estimated dynamics. Substituting either estimator directly into the controlled SDE (17) yields:

$$dX_t^* = \left[b_t(X_t^*) + \frac{\sigma_t^2}{2} \nabla \log p_t(X_t^*) + \sigma_t^2 \widehat{\nabla V_t(X_t^*)} \right] dt + \sigma_t dB_t, \quad X_0^* \sim p_0. \quad (38)$$

These dynamics can be simulated via the Euler-Maruyama scheme provided in Algorithm 6. Analogously, to enable ODE sampling, we apply the estimators to the probability flow ODE formulation (19) giving:

$$\dot{x}_t^* = b_t(x_t^*) + \frac{\sigma_t^2}{2} \widehat{\nabla V_t(x_t^*)}, \quad x_0^* \sim p_0. \quad (39)$$

We can integrate this ODE using any numerical integrator; we provide an Euler implementation in Algorithm 3.

Convergence guarantees. Even with an optimally trained MFM, the practical samplers (38) and (39) incur errors from both time discretization and Monte Carlo estimation of the optimal drift. Below we explicitly quantify these convergence rates for the SDE sampler.

Proposition 5.1 (Convergence Rates). *Let \hat{p}_1 denote the terminal distribution generated by the MFM steering (SDE) sampler (38) using K uniform Euler–Maruyama steps and N independent Monte Carlo samples per step. Under suitable regularity assumptions, the convergence to the target p_{reward} satisfies:*

$$W_2(\hat{p}_1, p_{\text{reward}}) \leq C \left(\frac{1}{\sqrt{K}} + \frac{1}{N} \right) \quad \text{and} \quad \text{KL}(\hat{p}_1 \| p_{\text{reward}}) \leq C \left(\frac{1}{K} + \frac{1}{N} \right), \quad (40)$$

for a constant $C > 0$ independent of K and N .

We provide a formal statement and proof in Appendix C.2. We note that the constant C depends exponentially on the dimension d . Additionally, while the KL bound relies on Girsanov’s theorem and is specific to the stochastic setting, a comparable W_2 bound holds for the ODE sampler through a similar stability analysis.

5.2 Training -Time Fine-Tuning

Besides inference-time steering, MFMs also facilitate efficient *training-time* alignment. Given a pretrained flow matching model b_t targeting p_1 (potentially extracted from an MFM), we can fine-tune a new model \hat{b}_t to permanently capture the optimal steering drift b_t^* defined in (19). This fine-tuned drift targets the reward-tilted distribution p_{reward} . Furthermore, this approach can be integrated into a self-distillation framework to directly learn the tilted flow map that compresses the trajectories of b_t^* into a one-step model (Boffi et al., 2025), or to be used for teacher-distillation (see Section 4.3.2) to train the corresponding tilted MFM. This extends the capabilities of MFMs beyond inference-time steering to enable permanent reward alignment of generative models.

We parametrize our fine-tuning network $\hat{b}_t : \mathbb{R}^d \rightarrow \mathbb{R}^d$ and seek an objective to learn b_t^* . A naive approach would be to regress \hat{b}_t directly onto the Monte Carlo drift estimators (20) or (22). However, these estimators are *self-normalized*—taking the form of a ratio of sample means—and therefore exhibit a small but non-zero bias for any finite number of Monte Carlo samples N . To circumvent this, we construct an unbiased objective by rearranging the definition of the optimal drift. Recall from (19) and (21) that:

$$b_t^*(x) = b_t(x) + \frac{\sigma_t^2}{2} \nabla V_t(x) = b_t(x) + \frac{\sigma_t^2}{2} \frac{\mathbb{E}_{\epsilon \sim p_0} [\nabla \exp(r(X_{0,1}(\epsilon; t, x)))]}{\mathbb{E}_{\epsilon \sim p_0} [\exp(r(X_{0,1}(\epsilon; t, x)))]}. \quad (41)$$

To ensure the learned drift \hat{b}_t matches the optimal b_t^* without computing the ratio explicitly, we multiply through by the denominator. This yields the following *implicit optimality condition*, which holds if and only if $\hat{b}_t(x) = b_t^*(x)$:

$$\mathbb{E}_{\epsilon \sim p_0} \left[\exp(r(X_{0,1}(\epsilon; t, x))) \left(\hat{b}_t(x) - b_t(x) \right) - \frac{\sigma_t^2}{2} \nabla \exp(r(X_{0,1}(\epsilon; t, x))) \right] = 0. \quad (42)$$

We can enforce this condition by minimizing a surrogate regression loss designed such that its gradient expectation vanishes exactly when the condition holds.

Unbiased fine-tuning objective (MFM-FT). The optimal steering drift b_t^* is recovered as the unique fixed point of the following objective:

$$\mathcal{L}(\hat{b}) := \int_0^1 \mathbb{E} \left[\left\| (\hat{b}_t(x) - b_t(x)) + (e^{r(X_{0,1}(\epsilon; t, x))} - 1) \text{sg}(\hat{b}_t(x) - b_t(x)) - \frac{\sigma_t^2}{2} \nabla e^{r(X_{0,1}(\epsilon; t, x))} \right\|^2 \right] dt, \quad (43)$$

where the expectation is taken over $\epsilon \sim p_0$ and where $x \in \mathbb{R}^d$ can be sampled from any distribution with full support. Here, $\text{sg}(\cdot)$ denotes the stop gradient operator.

Remarkably, notice that the MFM-FT objective in (43) is explicitly an off-policy objective. The loss is defined pointwise for any $t \in [0, 1]$ and $x \in \mathbb{R}^d$ and so we can sample these from any distribution. In practice, we sample x to be a draw from the interpolant I_t because this is simulation free and should cover the support where we care about learning. We emphasize that this is in contrast to many fine-tuning methods which rely on on-policy simulation, i.e., they must draw samples from the current model. We can also sample x using the current \hat{b}_t in order to sample x in the most important regions, but this is not necessary.

Algorithm 2 MFM Training (From Data)

Require: Initial parameters θ of \hat{v} .

- 1: **while** not converged **do**
- 2: Sample $I_0 \sim p_0$, $I_1 \sim p_1$, $t \sim \text{Unif}[0, 1]$
- 3: $I_t \leftarrow \alpha_t I_0 + \beta_t I_1$
- 4: Sample $\bar{I}_0 \sim p_0$, $s \sim \text{Unif}[0, u]$
- 5: $\bar{I}_s \leftarrow \alpha_s \bar{I}_0 + \beta_s I_1$
- 6: $\frac{d}{ds} \bar{I}_s \leftarrow \dot{\alpha}_s \bar{I}_0 + \dot{\beta}_s I_1$
- 7: # Monte Carlo estimate of losses
- 8: $\mathcal{L}_{\text{diag}} \leftarrow \|\hat{v}_{s,s}(\bar{I}_s; t, I_t) - \frac{d}{ds} \bar{I}_s\|^2$
- 9: Compute any self-distillation loss $\mathcal{L}_{\text{cons}}$ in Table 1
- 10: $\mathcal{L}_{\text{MFM}} \leftarrow \mathcal{L}_{\text{diag}} + \mathcal{L}_{\text{cons}}$
- 11: Compute $\nabla_{\theta} \mathcal{L}_{\text{MFM}}$
- 12: Minimize \mathcal{L}_{MFM} by gradient descent
- 13: **end while**
- 14: **return** θ

Algorithm 3 MFM Steering (ODE)

Require: Reward $r(x)$; MFM X ; times $0 = t_0 < \dots < t_K = 1$; MC batch size N .

- 1: Initialize $x_0 \sim p_0$
- 2: **for** $k = 0, \dots, K-1$ **do**
- 3: $dt \leftarrow t_{k+1} - t_k$
- 4: $\sigma_{t_k}^2 \leftarrow 2(\frac{\dot{\beta}_{t_k}}{\beta_{t_k}} \alpha_{t_k}^2 - \dot{\alpha}_{t_k} \alpha_{t_k})$
- 5: $b_{t_k}(x_{t_k}) \leftarrow v_{t_k, t_k}(x_{t_k}; 0, \vec{0})$ as in (36)
- 6: Sample iid $\epsilon^{(n)} \sim p_0$ for $n = 1, \dots, N$
- 7: $\hat{x}_1^{(n)} \leftarrow X_{0,1}(\epsilon^{(n)}, t_k, x_{t_k})$
- 8: Compute $\widehat{\nabla V_{t_k}(x_{t_k})}$ via (20) or (22)
- 9: $x_{t_{k+1}} \leftarrow x_{t_k} + dt \cdot b_{t_k}(x_{t_k}) + \frac{dt \cdot \sigma_{t_k}^2}{2} \widehat{\nabla V_{t_k}(x_{t_k})}$
- 10: **end for**
- 11: **return** x_1

6 Related Work

Inference-time alignment & steering. Inference-time methods aim to adapt the sampling dynamics of a fixed pretrained model to sample from the reward-tilted distribution p_{reward} . Existing approaches broadly fall into two categories: methods that aim to approximate the exact tilted dynamics, and particle-based methods that rely on resampling or search. For the first class, many methods can be seen as attempting to perform exact steering by approximating the true posterior distribution $p_{1|t}(\cdot|x)$ with a surrogate. One common heuristic is to approximate this posterior with a point mass (such as at the conditional expectation of data, i.e., the denoised estimate) and includes methods such as DPS (Chung et al., 2024), FreeDoM (Yu et al., 2023), MPGD (He et al., 2023), or unified frameworks based on a similar principle (Bansal et al., 2023; Ye et al., 2024). Other methods attempt to have a more refined approximation to this posterior, such as LGD (Song et al., 2023a), which approximates the posterior as a Gaussian centred at the posterior mean with a manually selected variance. While efficient, these approximations introduce significant bias and often fail to guide trajectories correctly in multimodal or non-linear settings where the mean does not represent a valid data sample (He et al., 2023).

Conversely, exact sampling methods such as Sequential Monte Carlo (SMC) reweight or resample trajectories to strictly target the tilted distribution (Wu et al., 2024; Skreta et al., 2025; Singhal et al., 2025). Although unbiased in principle, these methods require prohibitively large number of particles to avoid weight degeneracy and collapse (Snyder et al., 2008; Bickel et al., 2008). Recent search-based methods attempt to mitigate this by estimating intermediate rewards via explicit rollouts (Li et al., 2025; Zhang et al., 2025), but this still incurs a substantial computational cost per sampling step. We refer to Uehara et al. (2025) for an overview.

Few-step samplers. Our training scheme for MFMs leverage learning objectives from the literature on consistency models (Song et al., 2023c,b) and flow maps (Kim et al., 2024a; Frans et al., 2024; Geng et al., 2024, 2025b; Boffi et al., 2024, 2025; Sabour et al., 2025). However, unlike existing approaches, which aim to accelerate sampling, MFMs must provide access to cheap (one-step), differentiable samples from $p_{1|t}(\cdot|x)$, for all (t, x) to support efficient estimation of the tilted drift.

Posterior sampling. A critical bottleneck in exact steering is the need to efficiently sample from the conditional posterior $p_{1|t}(\cdot|x)$. Many prior works rely on trajectory rollouts of SDEs (Elat et al., 2023; Li et al., 2025; Zhang et al., 2025; Jain et al., 2025). Due to the inefficiencies of SDE sampling, recent work has introduced training-free methods to enable more efficient ODE samplers. In the case where the prior is Gaussian, GLASS Flows (Holderrieth et al., 2025) leverage the sufficient statistics of Gaussian integrals to reparameterize standard

pretrained models into transition samplers. However, this method still relies on solving expensive ODEs during inference. Unlike GLASS, MFM eliminate the need for this iterative integration. Alternative approaches explicitly learn these transitions during training. For instance, Distributional Diffusion (Bortoli et al., 2025) and Gaussian Mixture Flow Matching (Chen et al., 2025) train models to output posterior distributions directly via proper scoring rules or mixture approximations. While Distributional Diffusion also trains a stochastic flow map, training with scoring rules can be challenging to tune and scale. In particular, they were not successful in implementing their approach for ImageNet (64×64), while we show MFM scale successfully to ImageNet (256×256).

Value function estimation. We mention the closely related field of neural sampling. Neural samplers aim to generate samples from a target distribution p_1 given access only to its unnormalized density \tilde{p}_1 . These methods are related to steering algorithms as sampling can often be rephrased as modifying a process that targets a simple reference distribution p_{ref} and steering it to sample from p_1 by choosing the reward $r(x) = \log \tilde{p}_1(x) - \log p_{\text{ref}}(x)$. In this way, steering algorithms and neural samplers can often be repurposed for the reciprocal task. Many existing neural samplers approach sampling as a stochastic optimal control problem and therefore also require obtaining estimates of the value function and its gradient. Within this field, we highlight a class of methods that use gradient-free Monte Carlo estimators for these objects (Huang et al., 2021; Vargas et al., 2022; Akhoun-Sadegh et al., 2024). However, these methods do not have access to true data samples and so they cannot obtain posterior samples directly. As a result, they often suffer from high variance.

Generative fine-tuning. Beyond inference-time steering, permanent weight adaptation is another dominant strategy for alignment. Existing work broadly follows two paradigms: *(A) Reward maximization* such as D-Flow (Ben-Hamu et al., 2024) and DRaFT (Clark et al., 2024), that directly optimize the expected reward. However, this often leads to mode collapse and over-fitting (Goodhart’s Law) as the model collapses to a single high-reward mode rather than the true posterior; *(B) Distribution Matching* techniques aim to align the model with the reward-tilted distribution, preserving diversity. Notable examples include DEFT (Denker et al., 2025), Adjoint Matching (Domingo-Enrich et al., 2025), Tilt Matching (Potapchik et al., 2025) and diffusion variants of DPO (Wallace et al., 2023).

7 Experiments

In this section, we steer MFM using the MC estimators of the optimal drift presented in (20) (MFM-GF) and (22) (MFM-G) across a range of tasks. In Section 7.1, we present guidance experiments where we target a conditional posterior, namely for an inverse problem on 2D Gaussian Mixture Models (GMMs), and a multi-modal class-conditional sampling problem on MNIST. In Section 7.2, we scale the MFM framework to ImageNet, and present results on reward steering and fine-tuning. For detailed experiment descriptions, additional results and any hyper-parameters, please see Appendix F.

7.1 Guidance

7.1.1 Gaussian Mixture Models

We first steer a 2D GMM prior towards an inverse problem posterior, $p(x|y_{\text{obs}})$, governed by a linear observation likelihood, $p(y_{\text{obs}}|x) = \mathcal{N}(y_{\text{obs}}; Ax, \sigma^2 I)$, where A denotes the linear measurement operator. Note that this synthetic experiment admits an analytic posterior allowing us to directly assess the sampling fidelity of different steering procedures, and as such, serves as a proof-of-concept. We compare both of the MC estimators against Diffusion Posterior Sampling (DPS) (Chung et al., 2024) and SMC, namely the Twisted Diffusion Sampler (Wu et al., 2024), which uses the Tweedie’s estimates of the reward to define intermediate targets. Our steering schemes outperform DPS and TDS even with as few as $N = 2$ or 4 MC samples, with DPS significantly over-representing the largest mode (Figure 4).

Following Proposition 5.1, we also empirically observe a strong improvement in steering performance as the number of samples in the MC estimators of the drift is increased.

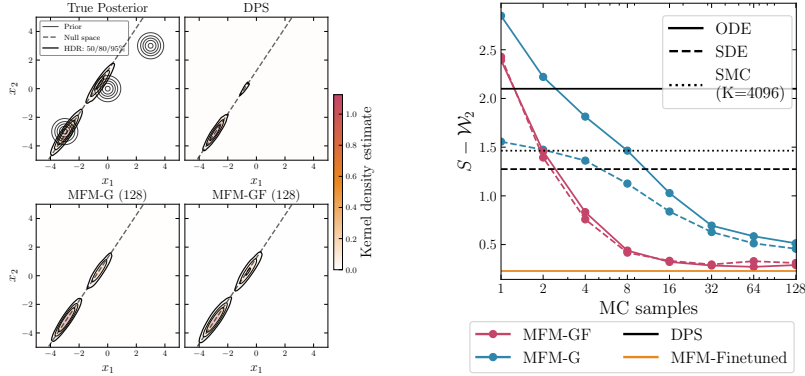


Figure 4 Comparison for GMM inverse problems. **Left** plot shows the prior, analytic posterior and density maps of posterior samples (ODE). **Center** graphs show the Sliced-Wasserstein, $S\text{-}\mathcal{W}_2$, between 4096 samples from the true posterior and our inference-time steering schemes. For SMC, we use $K = 4096$ particles, and report the mean $S\text{-}\mathcal{W}_2$ over 20 random seeds. **Right** table reports $S\text{-}\mathcal{W}_2$ and MMD for select inference-time steering set-ups and fine-tuning (ODE).

7.1.2 MNIST

We next consider a conditional sampling task with a highly-multimodal target on MNIST. We define a reward function as a weighted mixture of class probabilities obtained from a classifier: $\exp(r(x)) = p(c_{\text{mix}}|x) = \sum_{i=1}^C w_i p_\theta(y_i|x)$ where $p_\theta(y_i|x)$ denotes the classifier-predicted probability that image x belongs to class i , and the mixture weights w_i satisfy $\sum_{i=1}^C w_i = 1$. Note that by Bayes' rule,¹ the corresponding posterior distribution takes the form $p(x|c_{\text{mix}}) = \sum_{i=1}^C w_i p(x|y_i)$ which is a weighted mixture of class-conditional posteriors with weights w_i . By appropriately setting \mathbf{w} , we can define a challenging, highly multi-modal target distribution.

Consistent with the GMM experiments, DPS fails to respect the target class ratios, significantly over-representing the dominant mode. In contrast, both MFM-GF and MFM-G approach the correct target ratio as the number of MC samples increases. However, unlike the 2D GMM case, MFM-G significantly outperforms MFM-GF.

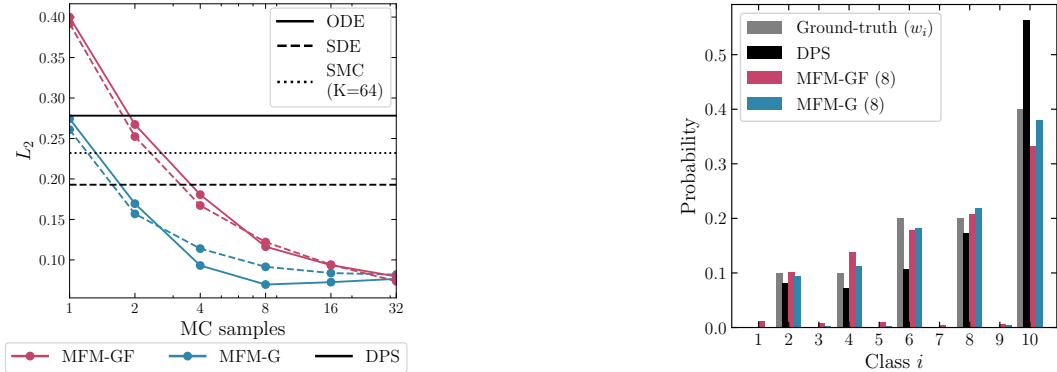


Figure 5 Comparison of the drift estimators through the empirical probability mass function (PMF) over the classes in the samples (from 4096 samples) and the ground-truth PMF of the target posterior (defined by the weight vector \mathbf{w}). **Left** graph shows the L_2 distance between the empirical PMF and ground-truth PMF for increasing number of MC samples. **Right** graph plots the ground-truth PMF, alongside the empirical PMF obtained through different drift estimators.

¹By Bayes' rule, $p(x|c_{\text{mix}}) = \sum_{i=1}^C p(x, y_i|c_{\text{mix}}) = \sum_{i=1}^C p(x|y_i, c_{\text{mix}}) p(y_i|c_{\text{mix}})$. If c_{mix} simply indexes the mixture, we identify $p(y_i|c_{\text{mix}}) = w_i$ and $p(x|y_i, c_{\text{mix}}) = p(x|y_i)$, yielding $p(x|c_{\text{mix}}) = \sum_{i=1}^C w_i p(x|y_i)$.

7.2 ImageNet

7.2.1 MFM Performance

We now consider ImageNet (256×256) (Deng et al., 2009) to evaluate the scalability of our framework. We provide training details and report the few-step performance of MFMs alongside deterministic few-step models.

Model. We use a standard latent Diffusion Transformer (DiT; Peebles et al. (2023)) operating in the latent space of a pre-trained Variational Auto-Encoder (VAE; Rombach et al. (2022)). We adapt the DiT architecture to accept the additional network inputs (t, x) required in MFMs with a minimal set of additional parameters (see Appendix B.2 for further details).

Training. We adapt DMF-XL/2+ (Lee et al., 2025), a state-of-the-art deterministic flow-map, and fine-tune it using the MFM distillation objective presented in Section 4.3. As the flow-map was trained using the Mean Flow objective, we leverage the Eulerian (Teacher) objective (see Table 1), the closest MFM distillation variant to Mean Flow, to avoid an unfavourable initialisation. We highlight that here we are distilling an MFM from a pre-trained flow model, and that this is not related to the reward fine-tuning objective in Equation 43. We present results for MFMs trained directly from data, including different model scales and ablations, in Appendix F.

Unconditional generation. Table 2 presents the performance of our model, MFM-XL/2, using the K -step refinement sampler (Algorithm 1). We achieve a competitive FID of **1.97** in just 4 steps, showing that MFMs are competitive with state-of-the-art deterministic baselines, while additionally providing stochastic one-step posterior samples for reward alignment.

Next, we evaluate the fidelity of the one and few-step posterior samplers, $p_{1|t}(\cdot|x_t)$, for different conditioning times, t (Figure 6). We compare to ODE rollouts of the conditional drift extracted from DMF XL/2+ using GLASS flows (Equation 25). Note that this is the source of diagonal supervision for MFM-XL/2, and as such, allows for a direct evaluation of the computational benefits of learning a one-step sampler. We consider two quantitative evaluations:

(A) Posterior recovery. We assess the fidelity of the posterior samples through FID. Concretely, we noise clean images to time t to form a conditioning set $\{x_t^{(i)}\}_{i=1}^N$ (where $N = 50,000$). For each noisy image, we generate a single posterior sample $\hat{x}_1^{(i)} \sim p(x_1 | x_t^{(i)})$ and compute the FID between the generated set $\{\hat{x}_1^{(i)}\}_{i=1}^N$ and 50,000 reference images from ImageNet. Both samplers are conditioned on the ground-truth class labels.

(B) Value function estimation. We evaluate the accuracy of Monte Carlo estimation of a value function, $V_t(x_t)$. We employ ImageReward (Xu et al., 2023) conditioned on the prompt “*A high-quality, high-resolution photograph of a tabby cat*” as the target reward. To establish a “ground truth” value estimate, we perform an expensive rollout of the SDE (200 steps) with $N = 200$ particles for a given noisy input x_t (derived from a *tabby cat* image). We then compute cheaper MC estimates using the same particle count ($N = 200$) but via the MFM or GLASS (ODE rollout) samplers. For both estimators, we condition the posterior samplers on the class *tabby cat*. We repeat for a set of x_t obtained through noising different images of tabby cats to time t , and compute the correlation between the high-fidelity estimator and the cheaper estimator.

As seen in Figure 6, MFMs strongly outperform explicit ODE rollouts across both posterior recovery and value function estimation, for all values of conditioning time and NFEs considered. Most notably, the relative

Deterministic Few-Step Flow Models			
Method	NFE	#Params	FID ↓
Shortcut-XL/2	1	676M	10.60
	4	676M	7.80
IMM-XL/2	2×1	676M	7.77
	2×2	676M	3.99
	2×4	676M	2.51
MF-XL/2+	1	676M	3.43
	2	676M	2.20
DMF-XL/2+	1	675M	2.16
	2	675M	1.64
	4	675M	1.51
Stochastic Few-Step Flow Models			
Method	NFE	#Params	FID ↓
MFM-XL/2	1	683M	3.72
	2	683M	2.40
	4	683M	1.97

Table 2 *ImageNet (256×256) benchmark.* $2 \times$ denotes usage of CFG. We compute FIDs using 50,000 generated and reference images.

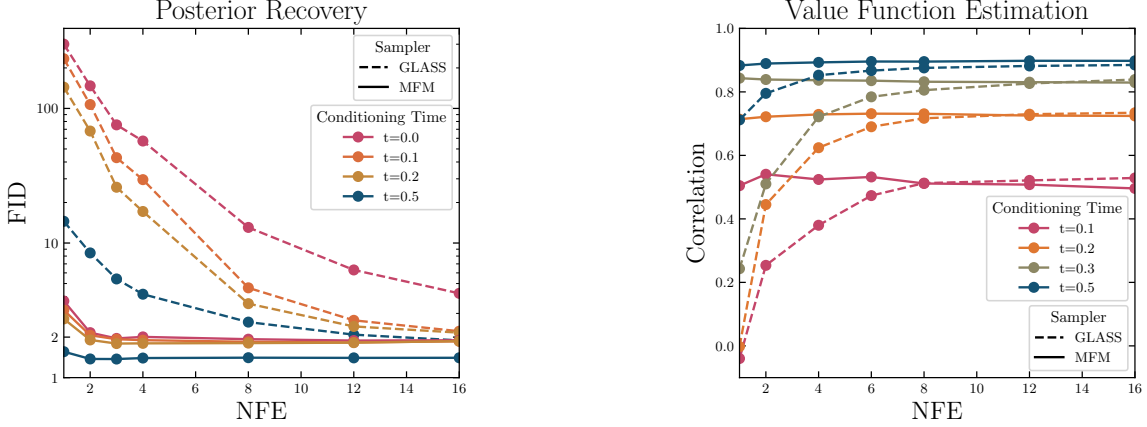


Figure 6 Comparison of the posterior samples from MFM XL/2 and GLASS flows for different conditioning times, t , and for increasing NFE. **Left** graph shows the posterior FID **Right** graph shows the correlation (Pearson’s r) between an expensive, high-fidelity MC estimator (SDE rollout) and an estimator obtained through MFM or GLASS flows.

improvement is greatest where the methods are limited to one function evaluation, which is of particular interest, as differentiating through rollouts to realise the gradient estimator in Equation 22 is prohibitively expensive.

7.2.2 Inference-Time Steering

Having demonstrated the substantial computational advantages of training MFMs for few-step posterior sampling, we now return to the core motivation: reward alignment. We begin by evaluating inference-time steering, where we steer the MFM XL/2 model using several text-to-image human preference reward models.

Experimental setup. We steer the class-conditioned ODE targetting class *tabby cat* using three different reward models, ImageReward (Xu et al., 2023), Pick Score (Kirstain et al., 2023), and HPSv2 (Wu et al., 2023) conditioned on the prompt “*A high-quality, high-resolution photograph of a tabby cat.*”. We also consider a range of reward multiplier values, $\lambda = \{1.0, 2.5, 5.0\}$, where $p_{\text{reward}}(x) \propto p_{\text{model}}(x) \exp(\lambda r_\theta(x, \text{prompt}))$. As in the conditional guidance experiments, we compare MFM-G and MFM-GF with DPS. We also consider the Best-of-N (BoN) baseline, which generates N_{BoN} samples and selects the highest reward sample. For each method, we generate 128 images, and compute the average reward. We provide further implementation details in Appendix F, including details on a simple, yet effective, rescaling of the magnitude of the steering gradient (Equation F.3.4) to combat discretization error.

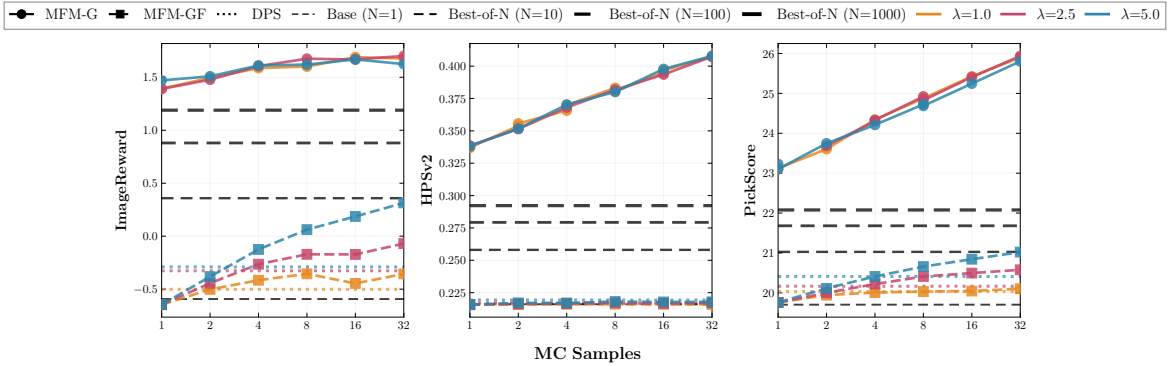


Figure 7 Performance comparison of MFM steering schemes against DPS and Best-of-N baselines employing ImageReward, HPSv2 and PickScore reward models.

Figure 7 highlights the effectiveness of steering using MFM-G, with it outperforming the Best-of-N variant with

$N = 1000$ across all models considered. We provide additional results in Appendix F, evaluating performance under reward models different from the one used for steering. This serves as a crucial check that the observed gains do not come at the expense of other related metrics, which would indicate reward hacking. Notably, steering with any of the three reward models does not degrade performance on the other metrics. In fact, when steering with either HPSv2 or PickScore, the resulting generations achieve higher scores on the other reward model than the Best-of-N baseline with $N = 1000$.

Computed-normalised performance. We next consider performance as a function of the number of function evaluations (NFEs). We present a detailed count of the NFEs required by each method in Appendix F.3.2. As shown in Figure 8, MFM-GF achieves substantially better compute-normalised performance than Best-of- N across all three reward models. In particular, its performance vs NFE curves lie strictly above those of Best-of- N . Notably, even the cheapest MFM-GF variant ($N = 1$) outperforms the most expensive Best-of- N configuration ($N_{\text{BoN}} = 1000$), while requiring $100\times$ fewer NFEs.

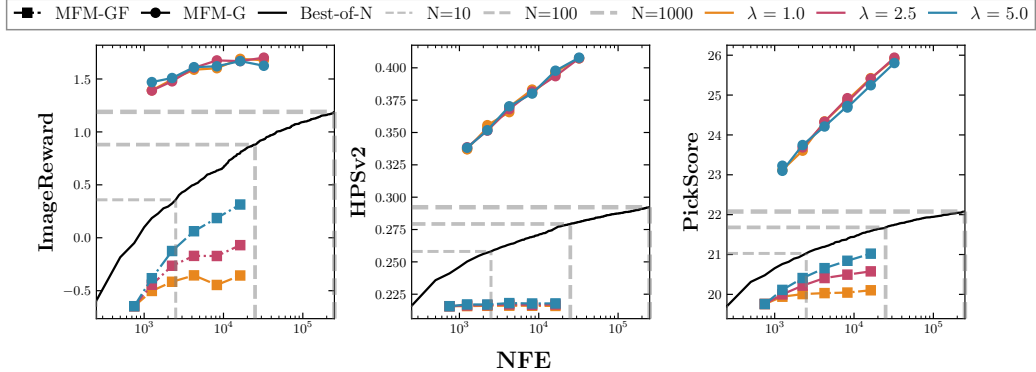


Figure 8 Compute-normalised performance comparison of MFM steering schemes and the Best-of- N baseline.



Figure 9 Base and steered (HPSv2) samples for 4 random seeds. These samples reinforce the quantitative inference-time scaling properties of MFM-GF in Figure 8, with the $N = 32$ variant producing visually more appealing images than $N = 1$. A larger set of samples can be found in Appendix F.

7.2.3 Fine-Tuning

Having established the effectiveness of inference-time steering at scale using MFMs, we now investigate fine-tuning the MFM using the objective in Equation 43. We design a fine-tuning procedure aimed at enhancing the general quality and fidelity of generated samples. To this end, we train across all the ImageNet classes using the HPSv2 reward model, conditioned on the prompt template "*A high-quality, high-resolution photograph of a {class}.*". We evaluate performance across a range of reward-multiplier values, $\lambda = \{10, 25, 50\}$ and present our results in Figure 10.

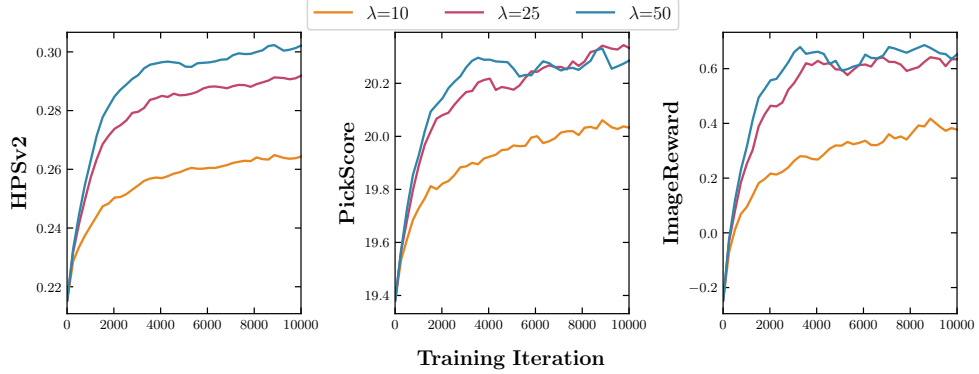


Figure 10 Reward metrics during reward fine-tuning with HPSv2. Rewards on HPSv2, ImageReward, and PickScore are computed every 500 training iterations and averaged across 512 ODE samples with the prompt template used during fine-tuning.

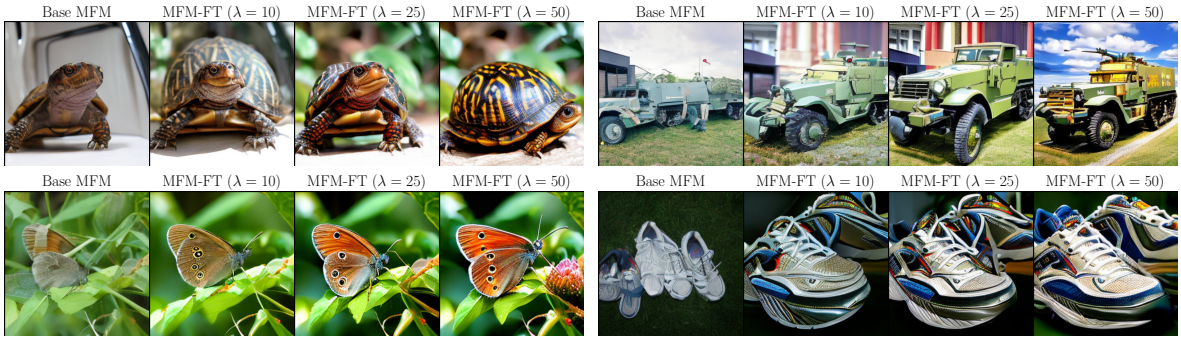


Figure 11 Samples from the class-conditioned ODE (250 steps) before and after fine-tuning using the MFM-FT objective for different values of λ , using the same seed.

Figure 10 demonstrates the effectiveness of the fine-tuning objective in Equation 43, with scores from all three reward models exhibiting a stable and consistent increase throughout fine-tuning on HPSv2. These improvements are also qualitatively reflected in the samples shown in Figure 11, where the fine-tuned MFMs produce visibly higher-quality and more colourful images while preserving the semantic content of the base MFM samples. We provide a larger set of samples in Appendix F.

8 Conclusion

We introduced Meta Flow Maps (MFMs), a framework for learning stochastic flow maps that efficiently generate samples from the family of conditional posteriors $p_{1|t}(\cdot|x)$. By amortizing the infinite family of conditional transport problems into a single few-step model, MFMs eliminate the computational bottleneck of explicit inner rollouts, enabling efficient, asymptotically exact inference-time steering. Beyond inference, we demonstrated that MFMs facilitate efficient, unbiased off-policy fine-tuning, allowing generative models to be permanently aligned with general rewards. Importantly, our framework is agnostic to the specific choice of training objective; future work can explore the rich design space of consistency losses and optimization techniques developed for deterministic flow maps to further enhance performance. Finally, we note that the MFM framework generalizes beyond fixed-endpoint generation to support arbitrary intermediate time prediction $p_{r|t}(\cdot|x)$, and extends to more general stochastic processes.

Acknowledgments

We thank Iskander Azangulov, Jakiw Pidstrigach, Sam Howard, Franklin Shiyi Wang, Yuyuan Chen, Carles Domingo-Enrich, Francisco Vargas, Peter Holderrieth, and George Deligiannidis for fruitful conversations. We also want to thank Arnaud Doucet in particular for his help with the theoretical development and for his suggestions on the paper. PP is supported by the EPSRC CDT in Modern Statistics and Statistical Machine Learning [EP/S023151/1], a Google PhD Fellowship, and an NSERC Postgraduate Scholarship (PGS D). AS is supported by the EPSRC CDT in Modern Statistics and Statistical Machine Learning [EP/Y034813/1]. AM is supported by the Clarendon Fund Scholarship, University of Oxford. AP is supported by the EPSRC and AstraZeneca via an iCASE award for a DPhil in Machine Learning. MSA is supported by a Junior Fellowship at the Harvard Society of Fellows as well as the National Science Foundation under Cooperative Agreement PHY-2019786 (The NSF AI Institute for Artificial Intelligence and Fundamental Interactions²). This work has been made possible in part by a gift from the Chan Zuckerberg Initiative Foundation to establish the Kempner Institute for the Study of Natural and Artificial Intelligence. The authors also acknowledge the use of resources provided by the Isambard-AI National AI Research Resource (AIRR) (McIntosh-Smith et al., 2024). Isambard-AI is operated by the University of Bristol and is funded by the UK Government’s Department for Science, Innovation and Technology (DSIT) via UK Research and Innovation; and the Science and Technology Facilities Council [ST/AIRR/I-A-I/1023].

References

- Tara Akhoud-Sadegh, Jarrid Rector-Brooks, Avishek Joey Bose, Sarthak Mittal, Pablo Lemos, Cheng-Hao Liu, Marcin Sendera, Siamak Ravanbakhsh, Gauthier Gidel, Yoshua Bengio, Nikolay Malkin, and Alexander Tong. 2024. Iterated denoising energy matching for sampling from boltzmann densities.
- Michael S Albergo, Nicholas M Boffi, and Eric Vanden-Eijnden. 2023a. Stochastic interpolants: A unifying framework for flows and diffusions. *arXiv preprint arXiv:2303.08797*.
- Michael S. Albergo, Mark Goldstein, Nicholas M. Boffi, Rajesh Ranganath, and Eric Vanden-Eijnden. 2023b. Stochastic interpolants with data-dependent couplings. *arXiv:2310.03725*.
- Michael S Albergo and Eric Vanden-Eijnden. 2022. Building normalizing flows with stochastic interpolants. In *The Eleventh International Conference on Learning Representations*.
- Brian D.O. Anderson. 1982. Reverse-time diffusion equation models. *Stochastic Processes and their Applications*, 12(3):313–326.
- Arpit Bansal, Hong-Min Chu, Avi Schwarzschild, Soumyadip Sengupta, Micah Goldblum, Jonas Geiping, and Tom Goldstein. 2023. Universal guidance for diffusion models.
- Heli Ben-Hamu, Omri Puny, Itai Gat, Brian Karrer, Uriel Singer, and Yaron Lipman. 2024. D-flow: Differentiating through flows for controlled generation.
- Peter Bickel, Bo Li, and Thomas Bengtsson. 2008. *Sharp failure rates for the bootstrap particle filter in high dimensions*, page 318–329. Institute of Mathematical Statistics.
- Nicholas M. Boffi, Michael S. Albergo, and Eric Vanden-Eijnden. 2024. Flow Map Matching: A unifying framework for consistency models. *arXiv:2406.07507*.
- Nicholas M. Boffi, Michael S. Albergo, and Eric Vanden-Eijnden. 2025. How to build a consistency model: Learning flow maps via self-distillation.
- Valentin De Bortoli, Alexandre Galashov, J. Swaroop Guntupalli, Guangyao Zhou, Kevin Murphy, Arthur Gretton, and Arnaud Doucet. 2025. Distributional diffusion models with scoring rules.
- Hansheng Chen, Kai Zhang, Hao Tan, Zexiang Xu, Fujun Luan, Leonidas Guibas, Gordon Wetzstein, and Sai Bi. 2025. Gaussian mixture flow matching models.
- Hyungjin Chung, Jeongsol Kim, Michael T. Mccann, Marc L. Klasky, and Jong Chul Ye. 2024. Diffusion posterior sampling for general noisy inverse problems.

²<http://iaifi.org/>

- Kevin Clark, Paul Vicol, Kevin Swersky, and David J Fleet. 2024. Directly fine-tuning diffusion models on differentiable rewards.
- Paolo Dai Pra. 1991. A stochastic control approach to reciprocal diffusion processes. *Applied Mathematics and Optimization*, 23(1):313–329.
- Jia Deng, Wei Dong, Richard Socher, Li-Jia Li, Kai Li, and Fei-Fei Li. 2009. Imagenet: a large-scale hierarchical image database. pages 248–255.
- Alexander Denker, Francisco Vargas, Shreyas Padhy, Kieran Didi, Simon Mathis, Vincent Dutordoir, Riccardo Barbano, Emile Mathieu, Urszula Julia Komorowska, and Pietro Lio. 2025. Deft: Efficient fine-tuning of diffusion models by learning the generalised h -transform.
- Prafulla Dhariwal and Alexander Nichol. 2021. Diffusion models beat gans on image synthesis. In *Advances in Neural Information Processing Systems*, volume 34, pages 8780–8794. Curran Associates, Inc.
- Carles Domingo-Enrich, Michal Drozdzal, Brian Karrer, and Ricky T. Q. Chen. 2025. Adjoint matching: Fine-tuning flow and diffusion generative models with memoryless stochastic optimal control.
- Noam Elata, Bahjat Kawar, Tomer Michaeli, and Michael Elad. 2023. Nested diffusion processes for anytime image generation.
- Kevin Frans, Danijar Hafner, Sergey Levine, and Pieter Abbeel. 2024. One step diffusion via shortcut models. *arXiv:2410.12557*.
- Kevin Frans, Danijar Hafner, Sergey Levine, and Pieter Abbeel. 2025. One step diffusion via shortcut models.
- Zhengyang Geng, Mingyang Deng, Xingjian Bai, J. Zico Kolter, and Kaiming He. 2025a. Mean flows for one-step generative modeling.
- Zhengyang Geng, Yiyang Lu, Zongze Wu, Eli Shechtman, J. Zico Kolter, and Kaiming He. 2025b. Improved mean flows: On the challenges of fastforward generative models.
- Zhengyang Geng, Ashwini Pokle, William Luo, Justin Lin, and J. Zico Kolter. 2024. Consistency Models Made Easy. *arXiv:2406.14548*.
- Yutong He, Naoki Murata, Chieh-Hsin Lai, Yuhta Takida, Toshimitsu Uesaka, Dongjun Kim, Wei-Hsiang Liao, Yuki Mitsufuji, J. Zico Kolter, Ruslan Salakhutdinov, and Stefano Ermon. 2023. Manifold preserving guided diffusion.
- Jonathan Ho, Ajay Jain, and Pieter Abbeel. 2020. Denoising diffusion probabilistic models. In *Advances in neural information processing systems*, volume 33, pages 6840–6851.
- Jonathan Ho and Tim Salimans. 2022. Classifier-free diffusion guidance. *arXiv preprint arXiv:2207.12598*.
- Peter Holderrieth, Uriel Singer, Tommi Jaakkola, Ricky T. Q. Chen, Yaron Lipman, and Brian Karrer. 2025. Glass flows: Transition sampling for alignment of flow and diffusion models.
- Jian Huang, Yuling Jiao, Lican Kang, Xu Liao, Jin Liu, and Yanyan Liu. 2021. Schrödinger-föllmer sampler: Sampling without ergodicity.
- Vineet Jain, Kusha Sareen, Mohammad Pedramfar, and Siamak Ravanbakhsh. 2025. Diffusion tree sampling: Scalable inference-time alignment of diffusion models.
- Tero Karras, Miika Aittala, Timo Aila, and Samuli Laine. 2022. Elucidating the design space of diffusion-based generative models. *arXiv:2206.00364*.
- Dongjun Kim, Yeongmin Kim, Se Jung Kwon, Wanmo Kang, and Il-Chul Moon. 2023. Refining generative process with discriminator guidance in score-based diffusion models.
- Dongjun Kim, Chieh-Hsin Lai, Wei-Hsiang Liao, Naoki Murata, Yuhta Takida, Toshimitsu Uesaka, Yutong He, Yuki Mitsufuji, and Stefano Ermon. 2024a. Consistency trajectory models: Learning probability flow ode trajectory of diffusion.
- Dongjun Kim, Chieh-Hsin Lai, Wei-Hsiang Liao, Naoki Murata, Yuhta Takida, Toshimitsu Uesaka, Yutong He, Yuki Mitsufuji, and Stefano Ermon. 2024b. Consistency Trajectory Models: Learning Probability Flow ODE Trajectory of Diffusion. *arXiv:2310.02279*.
- Diederik P. Kingma and Jimmy Ba. 2017. Adam: A method for stochastic optimization. *arXiv:1412.6980*.

- Diederik P Kingma and Max Welling. 2022. Auto-encoding variational bayes.
- Yuval Kirstain, Adam Polyak, Uriel Singer, Shahbuland Matiana, Joe Penna, and Omer Levy. 2023. Pick-a-pic: An open dataset of user preferences for text-to-image generation.
- Kyungmin Lee, Sihyun Yu, and Jinwoo Shin. 2025. Decoupled meanflow: Turning flow models into flow maps for accelerated sampling. *arXiv preprint arXiv:2510.24474*.
- Xiner Li, Masatoshi Uehara, Xingyu Su, Gabriele Scialia, Tommaso Biancalani, Aviv Regev, Sergey Levine, and Shuiwang Ji. 2025. Dynamic search for inference-time alignment in diffusion models.
- Yaron Lipman, Ricky TQ Chen, Heli Ben-Hamu, Maximilian Nickel, and Matthew Le. 2022. Flow matching for generative modeling. In *The Eleventh International Conference on Learning Representations*.
- Liyuan Liu, Haoming Jiang, Pengcheng He, Weizhu Chen, Xiaodong Liu, Jianfeng Gao, and Jiawei Han. 2021. On the variance of the adaptive learning rate and beyond.
- Xingchao Liu, Chengyue Gong, and Qiang Liu. 2022. Flow straight and fast: Learning to generate and transfer data with rectified flow. In *The Eleventh International Conference on Learning Representations*.
- Nanye Ma, Shangyuan Tong, Haolin Jia, Hexiang Hu, Yu-Chuan Su, Mingda Zhang, Xuan Yang, Yandong Li, Tommi Jaakkola, Xuhui Jia, and Saining Xie. 2025. Inference-time scaling for diffusion models beyond scaling denoising steps.
- Simon McIntosh-Smith, Sadaf Alam, and Christopher Woods. 2024. Isambard-ai: a leadership class supercomputer optimised specifically for artificial intelligence.
- William Peebles and Saining Xie. 2023. Scalable diffusion models with transformers. In *Proceedings of the IEEE/CVF International Conference on Computer Vision*, pages 4195–4205.
- Peter Potapchik, Cheuk-Kit Lee, and Michael S. Albergo. 2025. Tilt matching for scalable sampling and fine-tuning.
- Robin Rombach, Andreas Blattmann, Dominik Lorenz, Patrick Esser, and Björn Ommer. 2022. High-resolution image synthesis with latent diffusion models. In *Proceedings of the IEEE/CVF conference on computer vision and pattern recognition*, pages 10684–10695.
- Amirmojtaba Sabour, Sanja Fidler, and Karsten Kreis. 2025. Align your flow: Scaling continuous-time flow map distillation.
- Raghav Singhal, Zachary Horvitz, Ryan Teehan, Mengye Ren, Zhou Yu, Kathleen McKeown, and Rajesh Ranganath. 2025. A general framework for inference-time scaling and steering of diffusion models.
- Marta Skreta, Tara Akhound-Sadegh, Viktor Ohanesian, Roberto Bondesan, Alán Aspuru-Guzik, Arnaud Doucet, Rob Brekelmans, Alexander Tong, and Kirill Neklyudov. 2025. Feynman-kac correctors in diffusion: Annealing, guidance, and product of experts.
- Chris Snyder, Thomas Bengtsson, Peter Bickel, and Jeff Anderson. 2008. Obstacles to high-dimensional particle filtering. *Monthly Weather Review*, 136(12):4629 – 4640.
- Jiaming Song, Qinsheng Zhang, Hongxu Yin, Morteza Mardani, Ming-Yu Liu, Jan Kautz, Yongxin Chen, and Arash Vahdat. 2023a. Loss-guided diffusion models for plug-and-play controllable generation. In *International Conference on Machine Learning*, pages 32483–32498. PMLR.
- Yang Song and Prafulla Dhariwal. 2023b. Improved techniques for training consistency models.
- Yang Song, Prafulla Dhariwal, Mark Chen, and Ilya Sutskever. 2023c. Consistency models.
- Yang Song, Jascha Sohl-Dickstein, Diederik P Kingma, Abhishek Kumar, Stefano Ermon, and Ben Poole. 2020. Score-based generative modeling through stochastic differential equations. *arXiv:2011.13456*.
- Zhicong Tang, Jianmin Bao, Dong Chen, and Baining Guo. 2025. Diffusion models without classifier-free guidance. *arXiv preprint arXiv:2502.12154*.
- Masatoshi Uehara, Yulai Zhao, Chenyu Wang, Xiner Li, Aviv Regev, Sergey Levine, and Tommaso Biancalani. 2025. Inference-time alignment in diffusion models with reward-guided generation: Tutorial and review.
- Francisco Vargas, Andrius Ovsianas, David Fernandes, Mark Girolami, Neil D. Lawrence, and Nikolas Nüsken. 2022. Bayesian learning via neural schrödinger-föllmer flows.
- Bram Wallace, Meihua Dang, Rafael Rafailov, Linqi Zhou, Aaron Lou, Senthil Purushwalkam, Stefano Ermon, Caiming Xiong, Shafiq Joty, and Nikhil Naik. 2023. Diffusion model alignment using direct preference optimization.

- Luhuan Wu, Brian L. Trippe, Christian A. Naesseth, David M. Blei, and John P. Cunningham. 2024. Practical and asymptotically exact conditional sampling in diffusion models.
- Xiaoshi Wu, Yiming Hao, Keqiang Sun, Yixiong Chen, Feng Zhu, Rui Zhao, and Hongsheng Li. 2023. Human preference score v2: A solid benchmark for evaluating human preferences of text-to-image synthesis.
- Jiazheng Xu, Xiao Liu, Yuchen Wu, Yuxuan Tong, Qinkai Li, Ming Ding, Jie Tang, and Yuxiao Dong. 2023. Imagereward: Learning and evaluating human preferences for text-to-image generation.
- Haotian Ye, Haowei Lin, Jiaqi Han, Minkai Xu, Sheng Liu, Yitao Liang, Jianzhu Ma, James Zou, and Stefano Ermon. 2024. Tfg: Unified training-free guidance for diffusion models.
- Jiwen Yu, Yinhuai Wang, Chen Zhao, Bernard Ghanem, and Jian Zhang. 2023. Freedom: Training-free energy-guided conditional diffusion model.
- Xiangcheng Zhang, Haowei Lin, Haotian Ye, James Zou, Jianzhu Ma, Yitao Liang, and Yilun Du. 2025. Inference-time scaling of diffusion models through classical search.

Appendix

A	Methodology	25
A.1	Reparametrization	25
A.2	Short Flow Segments	26
A.3	Drift Reparametrization	26
A.4	Connection to γ -sampling	26
A.5	Extension to Arbitrary Prediction Times and General Stochastic Processes	27
B	Implementation Details	28
B.1	Model Guidance	28
B.2	Architecture	28
B.3	Adaptive Loss	29
C	Proofs	29
C.1	Conditional Endpoint Law	29
C.2	Convergence Guarantees	30
D	GLASS Flows (Holderrieth et al., 2025)	35
E	Algorithms	35
F	Experiment Details & Additional Results	36
F.1	Gaussian Mixture Model	36
F.2	MNIST	36
F.3	ImageNet (256 \times 256)	37

A Methodology

A.1 Reparametrization

Suppose that we have an MFM X trained on an interpolant $(I_t)_{t \in [0,1]}$ with coefficients α_t, β_t . We emphasize that here we do not necessarily assume that p_0 is Gaussian. We denote the marginal density of I_t by p_t and the conditionals posterior of I_1 given $I_t = x$ by $p_{1|t}(\cdot|x)$. We describe how this MFM can be reparametrized to sample from posteriors arising from interpolants with different coefficients. Let \tilde{I}_t be the interpolant defined by

$$\tilde{I}_t = \tilde{\alpha}_t I_0 + \tilde{\beta}_t I_1, \quad (44)$$

for some new coefficients $\tilde{\alpha}_t, \tilde{\beta}_t$. Let \tilde{p}_t be the marginal density of \tilde{I}_t and let $\tilde{p}_{1|t}(\cdot|x)$ denote the conditional posterior. Rearranging the interpolant definition, we have

$$\frac{1}{\tilde{\beta}_t} \tilde{I}_t = \frac{\tilde{\alpha}_t}{\tilde{\beta}_t} I_0 + I_1. \quad (45)$$

Since α_t and β_t are continuous in t and since the boundary conditions satisfy $\alpha_0 = 1, \beta_0 = 0$ and $\alpha_1 = 0, \beta_1 = 1$, this implies that the map $t \mapsto \frac{\alpha_t}{\beta_t}$ is a surjection from $[0, 1]$ onto $[0, \infty)$. Therefore there exists $t^* \in [0, 1]$ such that $\frac{\alpha_{t^*}}{\beta_{t^*}} = \frac{\dot{\alpha}_t}{\dot{\beta}_t}$ and for this t^* we have

$$\frac{1}{\tilde{\beta}_t} \tilde{I}_t = \frac{\alpha_{t^*}}{\beta_{t^*}} I_0 + I_1, \quad (46)$$

and so

$$\frac{\beta_{t^*}}{\tilde{\beta}_t} \tilde{I}_t = \alpha_{t^*} I_0 + \beta_{t^*} I_1. \quad (47)$$

In particular, this shows that

$$\tilde{p}_{1|t}(\cdot|x) = p_{1|t^*}(\cdot | \frac{\beta_{t^*}}{\tilde{\beta}_t} x). \quad (48)$$

Therefore, we can sample from the conditional posterior $\tilde{p}_{1|t}(\cdot|x)$ using the MFM X trained on the interpolant with coefficients α_t, β_t . In particular, if $\epsilon \sim p_0$, then

$$X_{0,1}(\epsilon; t^*, \frac{\beta_{t^*}}{\tilde{\beta}_t} x) \sim \tilde{p}_{1|t}(\cdot|x). \quad (49)$$

This means that we can obtain differentiable, one-shot samples from posteriors of this form even if our MFM was trained on a different interpolant path.

A.2 Short Flow Segments

In practice, we will often explicitly form $b_t(x)$ when performing Euler-style updates for an ODE or SDE simulation. As discussed in the main body, we can extract this drift from a trained MFM using (36). Another approach is to use short flow segments as follows:

$$\Delta t b_t(x) = X_{t,t+\Delta t}(x; 0, x_0) - x + \mathcal{O}(\Delta t^2), \quad (50)$$

which holds for any $x, x_0 \in \mathbb{R}^d$. Depending on the context, this may help reduce discretization errors.

A.3 Drift Reparametrization

In addition to the extraction in (36) another reparametrization that can be used to extract the unconditional drift b_t from an MFM X is given by

$$b_t(x_t) = \frac{\dot{\alpha}_t}{\alpha_t} x_t + \frac{\dot{\beta}_t - \frac{\dot{\alpha}_t}{\alpha_t} \beta_t}{\dot{\beta}_0} (v_{0,0}(x; t, x_t) - \dot{\alpha}_0 x), \quad (51)$$

which holds for any x and any x_t . This follows from the identities $b_t(x_t) = \frac{\dot{\alpha}_t}{\alpha_t} x_t + (\dot{\beta}_t - \frac{\dot{\alpha}_t}{\alpha_t} \beta_t) \mathbb{E}[I_1 | I_t = x_t]$ and $v_{0,0}(x, t, x_t) = \dot{\alpha}_0 x + \dot{\beta}_0 \mathbb{E}[I_1 | I_t = x_t]$.

A.4 Connection to γ -sampling.

We note that our K -step refinement sampler is similar to flow map γ -sampling (Kim et al., 2024b) with $\gamma = 1$. See Algorithm 5 for an implementation with MFMs. In particular, the difference is that step 4 of Algorithm 1 is replaced with

$$\hat{x}_1^{(k)} \leftarrow X_{t_k, 1}(x_{t_k}; 0, \vec{0}). \quad (52)$$

Similar as with the K -step refinement, we have that $\hat{x}_1^{(k)} \sim p_1$, so $x_{t_{k+1}}$ has marginal density $p_{t_{k+1}}$ for all k . However, the core difference is that γ -sampling employs marginal transport whereas the K -step refinement uses conditional transport to obtain the sample at time 1.

A.5 Extension to Arbitrary Prediction Times and General Stochastic Processes

The MFM construction generalizes beyond fixed-endpoint generation to support prediction at arbitrary intermediate times for stochastic processes defined over a general index set \mathcal{T} . One can learn MFMs to condition on multiple time points $\{t_i\}_{i=1}^M$, for simplicity, we detail the case of conditioning on one intermediate time t . Let $(X_t)_{t \in \mathcal{T}}$ be an arbitrary stochastic process; for example, (X_t) could represent frames in a video or a time series of weather data. We emphasize that this process need not be an interpolant or defined by a flow matching process. Fix a conditioning pair $(t, x) \in \mathcal{T} \times \mathbb{R}^d$ and a target prediction time $r \in \mathcal{T}$. We define the conditional distribution as

$$p_{r|t}(\cdot|x) := \text{Law}(X_r | X_t = x). \quad (53)$$

As in Section 4, we introduce a context-dependent drift $\bar{b}_s(\cdot; r, t, x)$ defined over an auxiliary flow time $s \in [0, 1]$. This drift is defined as the solution to a conditional flow matching problem that transports a simple base noise distribution q to the target posterior $p_{r|t}(\cdot|x)$. We choose the initial distribution of this auxiliary flow to be a tractable distribution q , such as a Gaussian. (Note that 0 may not be in the index set \mathcal{T} and even if it is, $p_0 = \text{Law}(X_0)$ is generally intractable to sample from during inference. This is why we choose a different base measure q .) This drift defines an auxiliary probability flow ODE

$$\frac{d}{ds} \bar{x}_s = \bar{b}_s(\bar{x}_s; r, t, x), \quad \bar{x}_0 \sim q \implies \text{Law}(\bar{x}_1) = p_{r|t}(\cdot|x). \quad (54)$$

We emphasize that the auxiliary flow $(\bar{x}_s)_{s \in [0,1]}$ does not reproduce the conditional physical evolution of the process (X_τ) from $\tau = t$ to $\tau = r$; instead, it serves strictly as a transport bridge constructed to satisfy the endpoint distributional constraint $\bar{x}_1 \sim p_{r|t}(\cdot|x)$. We define an *extended Meta Flow Map* $X_{s,u}(\cdot; r, t, x) : \mathbb{R}^d \rightarrow \mathbb{R}^d$ as the parametric solution operator for this infinite family of ODEs, satisfying

$$X_{s,u}(\bar{x}_s; r, t, x) = \bar{x}_u, \quad \forall s, u \in [0, 1], \quad (55)$$

where $(x_\tau)_{\tau \in [0,1]}$ are trajectories of (54). Consequently, X satisfies the property of an extended stochastic flow map

$$X_{0,1}(\cdot; r, t, x) \# q = p_{r|t}(\cdot|x), \quad \forall r, t \in \mathcal{T}, \forall x \in \mathbb{R}^d. \quad (56)$$

In practice, we parametrize the MFM in terms of the average velocity $v_{s,u}(\cdot; r, t, x) : \mathbb{R}^d \rightarrow \mathbb{R}^d$:

$$\hat{X}_{s,u}(\bar{x}; r, t, x) = \bar{x} + (u - s)v_{s,u}(\bar{x}; r, t, x). \quad (57)$$

Training requires minimizing a diagonal loss $\mathcal{L}_{\text{diag}}$ and a consistency loss $\mathcal{L}_{\text{cons}}$ over a neural parameterization $\hat{v}_{s,u}$. To train the diagonal, we sample coupled pairs (X_r, X_t) from a dataset of real trajectories and construct a reference interpolant

$$\bar{I}_s = \alpha_s \bar{I}_0 + \beta_s Y_r, \quad \bar{I}_0 \sim q. \quad (58)$$

The flow matching loss is evaluated by regressing the learned velocity onto the time derivative $\frac{d}{ds} \bar{I}_s = \dot{\alpha}_s \bar{I}_0 + \dot{\beta}_s Y_r$, amortized over the index set \mathcal{T} :

$$\mathcal{L}_{\text{diag}}(\hat{v}) := \int_{\mathcal{T}} \int_{\mathcal{T}} \int_0^1 \mathbb{E} \left[\left| \hat{v}_{s,s}(\bar{I}_s; r, t, Y_t) - \frac{d}{ds} \bar{I}_s \right|^2 \right] ds d\mu(t) d\mu(r), \quad (59)$$

where μ is a measure on \mathcal{T} (such as the uniform distribution). Minimizing $\mathcal{L}_{\text{diag}}(\hat{v})$ ensures that

$$\hat{v}_{s,s}(\bar{x}; r, t, x) = \mathbb{E} \left[\frac{d}{ds} \bar{I}_s \mid \bar{I}_s = \bar{x}, X_t = x \right] = \mathbb{E} \left[\dot{\alpha}_s \bar{I}_0 + \dot{\beta}_s Y_r \mid \bar{I}_s = \bar{x}, X_t = x \right] = \bar{b}_s(\bar{x}; r, t, x). \quad (60)$$

Consistency is enforced by applying any standard consistency objective, such as those in Table 1, to the conditional map $\hat{X}_{s,u}$, where the loss is augmented by passing the target time r and conditioning state (t, X_t) as additional inputs to the network.

B Implementation Details

B.1 Model Guidance

Classifier-Free Guidance (CFG) interpolates between conditional and unconditional velocities at inference-time, requiring two function evaluations for every denoising step (Ho et al., 2022):

$$\tilde{v}_\theta(x_t, t, y) = v_\theta(x_t, t, y) + \omega_{CFG} \cdot (v_\theta(x_t, t, y) - v_\theta(x_t, t, \emptyset)) \quad (61)$$

Tang et al. (2025) recently proposed Model Guidance (MG) to learn this interpolated velocity during training, in order to reduce the inference cost from two to one model evaluation per denoising step. This approach has been shown to be particularly effective for achieving competitive one and few-step performance (Geng et al., 2025a; Lee et al., 2025). The standard training objective for MG replaces the base class-conditioned drift with a target that leverages the model’s current conditional and unconditional drift estimates, as well as the class-conditioned velocity from data:

$$v^{\text{tgt}}(I_t, t, y) = \dot{I}_t + \omega \cdot \text{sg}(v_\theta(I_t, t, y) - v_\theta(I_t, t, \emptyset)) \quad (62)$$

where $\omega \in (0, 1)$ is the model guidance scale. The stop-gradient operator, denoted as $\text{sg}(\cdot)$, ensures training stability. By considering the fixed point of this objective, it is easy to show that this training target is equivalent to using a standard CFG scale of $\omega_{CFG} = 1/(1 - \omega)$ during sampling.

For MFM, we extend MG by conditioning on an arbitrary pair (t, x) along the stochastic interpolant. To this end, aligning with notation in Equation 31, the MFM training target becomes:

$$v_{s,s}^{\text{tgt}}(\bar{I}_s; t, I_t, y) = \frac{d}{ds} \bar{I}_s + \omega \cdot \text{sg}(\hat{v}_{s,s}(\bar{I}_s; t, I_t, y) - \hat{v}_{s,s}(\bar{I}_s; t, I_t, \emptyset)) \quad (63)$$

Recent works also consider amortizing over a range of ω values to allow further flexibility at inference time by passing an additional input ω to the network (Geng et al., 2025b). Through minimizing this objective on the diagonal, alongside a consistency objective of choice, we enable 1-NFE generation that recovers the desired CFG/MG distribution for all (t, x) . We leverage MG for training MFM models on ImageNet. Parameter choices are specified in Table 5.

B.2 Architecture

We leverage standard diffusion and flow architectures (Karras et al., 2022; Peebles et al., 2023) with extensions to accommodate the additional network inputs. For our ImageNet experiments, we use Diffusion Transformer (DiT) backbone following related works (Geng et al., 2025a; Lee et al., 2025). While we retain the core transformer blocks, we introduce two specific embedding mechanisms to condition standard architectures for flow maps, $\hat{X}_{s,u}(\cdot)$, on the outer flow time t and the corresponding state x , to yield a MFM, $\hat{X}_{s,u}(\cdot; t, x)$

In DiT-based flow maps, a global conditioning vector c , which is a function of start and endpoint times, s, u , and any additional conditioning signals, e.g. class, is used throughout the network. For MFM, we extend this vector to also incorporate outer-time t . In order to condition on the spatial state x , we introduce an additional patch embedder layer. We then form the input to the DiT as a combination of the inner-state, x_s , and outer conditioning state, x modulated by AdaLN-Zero conditioned on t :

$$c = \underbrace{\text{Embed}_{\text{time},s}(s) + \text{Embed}_{\text{time},u}(u) + \text{Embed}_{\text{class}}(y)}_{\text{Flow map}} + \underbrace{\text{Embed}_{\text{time},t}(t)}_{\text{MFM}} \quad (64)$$

$$x_{\text{input}} = \underbrace{\text{PatchEmbed}(x_s) + \text{PosEmbed}}_{\text{Flow map}} + \underbrace{\text{AdaLN-Zero}[\text{PatchEmbed}'(x)|t]}_{\text{MFM}} \quad (65)$$

Fine-tuning from a flow map For fine-tuning from a flow map, the flow map can be preserved at initialisation through zero initialisation of the t time embedding MLP, and ensuring the new AdaLN-Zero modulates the contribution of x to an all zero tensor.

Inductive bias at $t = 0$ As highlighted in Section 4.5, $p_{1|0}(\cdot|x_0) = p_1$ for any x_0 , meaning the conditional velocities and maps should in fact be independent of x_t at $t = 0$. As such, architectures that ensure that x is ignored by design at $t = 0$ (and diminished at low t) can be considered to improve performance.

The limited parameter and architectural overhead allows MFM to be implemented into popular generative modelling workflows and codebases.

B.3 Adaptive Loss

In our ImageNet experiments, we follow Mean Flow (Geng et al., 2025a) and use an adaptive loss for both the diagonal and consistency terms of the MFM loss (Equation 33). The adaptively weighted loss is $\text{sg}(w) \cdot \mathcal{L}$, with $\mathcal{L} = \|\Delta\|_2^2$, where $\|\Delta\|$ denotes the regression error. The weights are set as follows:

$$w = \frac{1}{(\|\Delta\|_2^2 + c)^p}, \quad (66)$$

where $c > 0$ and $p > 0$ are hyper-parameters. Note that $p = 0, c = 0$ recovers the standard \mathcal{L}_2 loss. See Table 4 for further results on different choices of these parameters.

C Proofs

C.1 Conditional Endpoint Law

Proposition C.1. *Assume $I_0 \sim p_0 = \mathcal{N}(0, I)$ and consider the interpolant*

$$I_t = \alpha_t I_0 + \beta_t I_1, \quad (67)$$

with $\alpha_0 = \beta_1 = 1$ and $\alpha_1 = \beta_0 = 0$, and . Define

$$\frac{\sigma_t^2}{2} = \frac{\dot{\beta}_t}{\beta_t} \alpha_t^2 - \dot{\alpha}_t \alpha_t, \quad (68)$$

and let $p_t = \text{Law}(I_t)$. Consider the SDE

$$dX_t = f_t(X_t)dt + \sigma_t dB_t, \quad f_t(x) = b_t(x) + \frac{\sigma_t^2}{2} \nabla \log p_t(x), \quad X_0 \sim p_0, \quad (69)$$

where

$$b_t(x) = \mathbb{E}[\dot{I}_t | I_t = x]. \quad (70)$$

Then for all $t \in [0, 1]$ and $x \in \mathbb{R}^d$

$$\text{Law}(X_1 | X_t = x) = \text{Law}(I_1 | I_t = x). \quad (71)$$

Proof. Note that $\text{Law}(X_t) = p_t$, see Song et al. (2020); Albergo et al. (2023b). Therefore the time reversal $(Y_t)_{t \in [0, 1]} := (X_{1-t})_{t \in [0, 1]}$ satisfies the following SDE (Anderson, 1982)

$$dY_t = \tilde{f}_{1-t}(Y_t) + \sigma_{1-t} dB_t, \quad \tilde{f}_t(x) = -b_t(x) + \frac{\sigma_t^2}{2} \nabla \log p_t(x), \quad Y_0 \sim p_1. \quad (72)$$

By Tweedie's formula we have the identity

$$\nabla \log p_t(x) = \frac{-x + \beta_t \mathbb{E}[I_1 | I_t = x]}{\alpha_t^2}. \quad (73)$$

This gives

$$\tilde{f}_t(x) = -\dot{\alpha}_t \mathbb{E}[I_0 | I_t = x] - \dot{\beta}_t \mathbb{E}[I_1 | I_t = x] + \left(\frac{\dot{\beta}_t}{\beta_t} \alpha_t^2 - \dot{\alpha}_t \alpha_t \right) \frac{-x + \beta_t \mathbb{E}[I_1 | I_t = x]}{\alpha_t^2} \quad (74)$$

$$= -\dot{\alpha}_t \mathbb{E}[I_0 | I_t = x] - \frac{\dot{\alpha}_t}{\alpha_t} \beta_t \mathbb{E}[I_1 | I_t = x] + \left(\frac{\dot{\alpha}_t}{\alpha_t} - \frac{\dot{\beta}_t}{\beta_t} \right) x. \quad (75)$$

Using the relation $x = \alpha_t \mathbb{E}[I_0 | I_t = x] + \beta_t \mathbb{E}[I_1 | I_t = x]$ we obtain

$$\tilde{f}_t(x) = -\frac{\dot{\beta}_t}{\beta_t} x. \quad (76)$$

We use an integrating factor. Let $\Phi(t) = \int_0^t -\frac{\dot{\beta}_{1-s}}{\beta_{1-s}} ds = \log \beta_{1-t}$ and by Ito's formula we have

$$d(e^{-\Phi(t)} Y_t) = -\Phi'(t) e^{-\Phi(t)} Y_t dt + e^{-\Phi(t)} dY_t \quad (77)$$

$$= \frac{\dot{\beta}_{1-t}}{\beta_{1-t}} e^{-\Phi(t)} Y_t dt - e^{-\Phi(t)} \frac{\dot{\beta}_{1-t}}{\beta_{1-t}} Y_t dt + e^{-\Phi(t)} \sigma_{1-t} dB_t \quad (78)$$

$$= e^{-\Phi(t)} \sigma_{1-t} dB_t. \quad (79)$$

Therefore

$$Y_t = e^{\Phi(t)} Y_0 + e^{\Phi(t)} \int_0^t e^{-\Phi(s)} \sigma_{1-s} dB_s. \quad (80)$$

Notice that $\int_0^t e^{-\Phi(s)} \sigma_{1-s} dB_s$ is a mean zero Gaussian with variance equal to

$$\int_0^t e^{-2\Phi(s)} \sigma_{1-s}^2 ds = \int_0^t 2\beta_{1-s}^{-2} \left(\frac{\dot{\beta}_{1-s}}{\beta_{1-s}} \alpha_{1-s}^2 - \dot{\alpha}_{1-s} \alpha_{1-s} \right) ds \quad (81)$$

$$= \int_0^t \frac{d}{ds} \left(\frac{\alpha_{1-s}^2}{\beta_{1-s}^2} \right) ds \quad (82)$$

$$= \frac{\alpha_{1-t}^2}{\beta_{1-t}^2}. \quad (83)$$

Therefore

$$\text{Law}(Y_t | Y_0) = \text{Law}(\alpha_{1-t} Z + \beta_{1-t} Y_0 | Y_0), \quad (84)$$

for some $Z \sim \mathcal{N}(0, I)$ independent of Y_0 . Since Y is the time reversal of X , we have for all $t \in [0, 1]$ and $x \in \mathbb{R}^d$

$$\text{Law}(X_t | X_1 = x) = \text{Law}(\alpha_t Z + \beta_t I_1 | x), \quad (85)$$

where $Z \sim \mathcal{N}(0, I)$ is independent of I_1 . Moreover, we also have equality of the marginal laws $\text{Law}(X_1) = \text{Law}(I_1)$, so the joint laws of the SDE and the interpolant coincide:

$$\text{Law}(X_t, X_1) = \text{Law}(I_t, I_1). \quad (86)$$

Equality of the joint laws implies equality of the corresponding conditional laws for all $t \in [0, 1]$ and $x \in \mathbb{R}^d$

$$\text{Law}(X_1 | X_t = x) = \text{Law}(I_1 | I_t = x), \quad (87)$$

which is precisely the desired claim. \square

C.2 Convergence Guarantees

In this section, we provide a proof for the convergence rates stated in Proposition 5.1 in the main text.

Proposition C.2 (Formal Convergence Guarantees). *Let p_{reward} denote the target distribution defined in (13). Let \hat{p}_1 denote the terminal distribution generated by the MFM steering (SDE) sampler (Algorithm 6) using a uniform time discretization with K steps ($t_k = k/K$) and N independent Monte Carlo samples per step.*

Suppose the following regularity conditions hold:

1. The reward function $r \in C^1(\mathbb{R}^d)$ and its gradient ∇r are both bounded.
2. The MFM $f(\epsilon, t, x) \in C^1(\mathbb{R}^d)$ in x and $\nabla_x f$ is bounded.

3. The optimal drift $b_t^*(x)$ is L -Lipschitz continuous in space and $1/2$ -Hölder continuous in time. That is, for all $t, s \in [0, 1]$ and $x, y \in \mathbb{R}^d$:

$$|b_t^*(x) - b_t^*(y)| \leq L|x - y| \quad \text{and} \quad |b_t^*(x) - b_s^*(x)| \leq C_{\text{time}}|t - s|^{1/2}. \quad (88)$$

4. There exist $\sigma_{\max} > \sigma_{\min} > 0$ such that $\sigma_{\min} \leq \sigma_t \leq \sigma_{\max}$ for all $t \in [0, 1]$.

Then, there exists a constant $C > 0$ independent of K and N such that the convergence to the target satisfies:

$$W_2(\hat{p}_1, p_{\text{reward}}) \leq C \left(\frac{1}{\sqrt{K}} + \frac{1}{N} \right) \quad \text{and} \quad \text{KL}(\hat{p}_1 \| p_{\text{reward}}) \leq C \left(\frac{1}{K} + \frac{1}{N} \right). \quad (89)$$

Remark C.3. We note that the regularity conditions on the drift may be violated at $t = 1$ if the target distribution is supported on a low-dimensional manifold, as the score function becomes singular. Following standard practice in diffusion theory, our results formally apply to the process stopped at $t = 1 - \varepsilon$ for a small $\varepsilon > 0$, where the score is smooth and the Lipschitz constant L_ε is finite. In the case of the Wasserstein bound, we pick up an additional term $W_2(p_{1-\varepsilon}, p_{\text{reward}})$ corresponding to the smoothing error, which allows us to bound the distance to the exact target.

Proof. To analyze the convergence, we view the discrete sampling algorithm (Algorithm 6) as a continuous-time randomized Euler scheme by interpolating the discrete algorithm. Let $t_k = k/K$ for $k = 0, \dots, K$ be a uniform time grid with step size $\delta = 1/K$. We define the randomized interpolant \hat{X}_t as the continuous process satisfying:

$$d\hat{X}_t = \hat{b}_{\eta(t)}^{(N)}(\hat{X}_{\eta(t)})dt + \sigma_t dB_t, \quad \hat{X}_0 \sim p_0, \quad (90)$$

where $\eta(t) = t_k$ for $t \in [t_k, t_{k+1})$. The drift $\hat{b}_{t_k}^{(N)}(x)$ is the Monte Carlo estimator of the optimal drift derived using N independent samples. Crucially, for each step k , we draw a fresh batch of N samples $\epsilon^{(k,1)}, \dots, \epsilon^{(k,N)} \sim p_0$ to construct the estimator. We use the Gradient Estimator defined in (22) for the drift. Specifically, $\hat{b}_t^{(N)}(x)$ estimates the optimal drift $b_t^*(x) = b_t(x) + \frac{\sigma_t^2}{2} \nabla \log p_t(x) + \sigma_t^2 \nabla V_t(x)$. Using the reparameterization $f(\epsilon, t, x) = \Phi_{0,1}(\epsilon; t, x)$, the gradient estimator is:

$$\hat{b}_t^{(N)}(x) = b_t(x) + \frac{\sigma_t^2}{2} \nabla \log p_t(x) + \sigma_t^2 \nabla_x \log \left(\frac{1}{N} \sum_{i=1}^N e^{r(f(\epsilon^{(i)}, t, x))} \right). \quad (91)$$

We compare \hat{X}_t to the optimal steered process X_t^* governed by the exact drift $b_t^*(x)$:

$$dX_t^* = b_t^*(X_t^*)dt + \sigma_t dB_t, \quad X_0^* \sim p_0. \quad (92)$$

Our main analysis relies on controlling the error of the Monte Carlo drift estimator. The following proposition establishes the bias and variance bounds that will be central to our main proof.

Proposition C.4 (Drift Estimator Moments). *There exists a constant C' such that for any x :*

$$\underbrace{\mathbb{E}[\hat{b}_t^{(N)}(x)] - b_t^*(x)}_{\text{Bias}} \leq \frac{C'}{N}, \quad \underbrace{\mathbb{E}\left[\left|\hat{b}_t^{(N)}(x) - \mathbb{E}[\hat{b}_t^{(N)}(x)]\right|^2\right]}_{\text{Variance}} \leq \frac{C'}{N}. \quad (93)$$

Proof. Recall that the estimator is given by $\hat{b}_t^{(N)}(x) = b_t(x) + \frac{\sigma_t^2}{2} \nabla \log p_t(x) + \sigma_t^2 \widehat{\nabla V}_t(x)$, where $b_t(x) + \frac{\sigma_t^2}{2} \nabla \log p_t(x)$ is deterministic. Therefore, the bias and variance of $\hat{b}_t^{(N)}(x)$ are determined by the properties of the gradient estimator $\widehat{\nabla V}_t(x)$. Recall that $\nabla V_t(x) = \frac{\mathbb{E}[e^{r(f(\epsilon, t, x))} \nabla_x(r \circ f)(\epsilon, t, x)]}{\mathbb{E}[e^{r(f(\epsilon, t, x))}]}$. The estimator takes the form of a ratio of sample means $\frac{\bar{G}}{W} = \frac{\frac{1}{N} \sum G_i}{\frac{1}{N} \sum W_i}$, where $W_i = e^{r(f(\epsilon^{(i)}, t, x))}$ and $G_i = W_i \nabla(r \circ f)(\epsilon^{(i)}, t, x)$. Let $\mu_W = \mathbb{E}[W_i]$ and $\mu_G = \mathbb{E}[G_i]$. The target is $\frac{\mu_G}{\mu_W}$. To analyze the bias and variance, we apply the multivariate Taylor expansion of the function $h(u, v) = u/v$ around the point (μ_G, μ_W) . The partial derivatives evaluated at the mean are:

$$\frac{\partial h}{\partial u} = \frac{1}{\mu_W}, \quad \frac{\partial h}{\partial v} = -\frac{\mu_G}{\mu_W^2}, \quad \frac{\partial^2 h}{\partial u^2} = 0, \quad \frac{\partial^2 h}{\partial v^2} = \frac{2\mu_G}{\mu_W^3}, \quad \frac{\partial^2 h}{\partial u \partial v} = -\frac{1}{\mu_W^2}. \quad (94)$$

Bias Analysis. Expanding $h(\bar{G}, \bar{W}) = \frac{\bar{G}}{\bar{W}}$ to the second order yields:

$$\frac{\bar{G}}{\bar{W}} = \frac{\mu_G}{\mu_W} + \frac{1}{\mu_W}(\bar{G} - \mu_G) - \frac{\mu_G}{\mu_W^2}(\bar{W} - \mu_W) \quad (95)$$

$$+ \frac{1}{2} \left[\frac{2\mu_G}{\mu_W^3}(\bar{W} - \mu_W)^2 - \frac{2}{\mu_W^2}(\bar{G} - \mu_G)(\bar{W} - \mu_W) \right] + R_3, \quad (96)$$

where R_3 is the remainder term. Taking the expectation, the first-order terms vanish since $\mathbb{E}[\bar{G}] = \mu_G$ and $\mathbb{E}[\bar{W}] = \mu_W$. For the second-order terms, we utilize the properties of the sample mean variances and covariances:

$$\mathbb{E}[(\bar{W} - \mu_W)^2] = \frac{1}{N} \text{Var}(W_i), \quad \mathbb{E}[(\bar{G} - \mu_G)(\bar{W} - \mu_W)] = \frac{1}{N} \text{Cov}(G_i, W_i). \quad (97)$$

Substituting these into the expectation:

$$\mathbb{E} \left[\frac{\bar{G}}{\bar{W}} \right] - \frac{\mu_G}{\mu_W} = \frac{1}{N} \left(\frac{\mu_G}{\mu_W^3} \text{Var}(W_i) - \frac{1}{\mu_W^2} \text{Cov}(G_i, W_i) \right) + \mathbb{E}[R_3]. \quad (98)$$

By our boundedness assumptions, W_i and G_i have bounded moments, and $\mu_W > 0$. The expectation of the remainder $\mathbb{E}[R_3]$ is dominated by third-order central moments of the sample means, which scale as $\mathcal{O}(N^{-2})$ for i.i.d. variables with bounded moments. Thus, the bias is dominated by the $1/N$ term:

$$\left| \mathbb{E}[\hat{b}_t^{(N)}(x)] - b_t^*(x) \right| \leq \frac{C'}{N}. \quad (99)$$

Variance Analysis. Using the second-order Taylor expansion of h around (μ_G, μ_W) , we have:

$$\frac{\bar{G}}{\bar{W}} = \frac{\mu_G}{\mu_W} + \mathcal{L} + R_2, \quad (100)$$

where $\mathcal{L} = \frac{1}{\mu_W}(\bar{G} - \mu_G) - \frac{\mu_G}{\mu_W^2}(\bar{W} - \mu_W)$ is the first-order linear term and R_2 is the remainder. Since $\mathbb{E}[\mathcal{L}] = 0$, the expectation of the estimator is

$$\mathbb{E} \left[\frac{\bar{G}}{\bar{W}} \right] = \frac{\mu_G}{\mu_W} + \mathbb{E}[R_2]. \quad (101)$$

Substituting this into the variance definition:

$$\text{Var} \left(\frac{\bar{G}}{\bar{W}} \right) = \mathbb{E} \left[\left(\left(\frac{\mu_G}{\mu_W} + \mathcal{L} + R_2 \right) - \left(\frac{\mu_G}{\mu_W} + \mathbb{E}[R_2] \right) \right)^2 \right] \quad (102)$$

$$= \mathbb{E}[(\mathcal{L} + (R_2 - \mathbb{E}[R_2]))^2] \quad (103)$$

$$= \mathbb{E}[\mathcal{L}^2] + 2\mathbb{E}[\mathcal{L}(R_2 - \mathbb{E}[R_2])] + \text{Var}(R_2). \quad (104)$$

The dominant term is the variance of the linear approximation $\mathbb{E}[\mathcal{L}^2]$:

$$\mathbb{E}[\mathcal{L}^2] = \frac{1}{N} \left(\frac{\text{Var}(G_i)}{\mu_W^2} + \frac{\mu_G^2 \text{Var}(W_i)}{\mu_W^4} - \frac{2\mu_G \text{Cov}(G_i, W_i)}{\mu_W^3} \right). \quad (105)$$

The other terms involve the remainder R_2 , which scales as $\mathcal{O}(N^{-1})$. Therefore, the cross-term $\mathbb{E}[\mathcal{L}R_2]$ and $\text{Var}(R_2)$ scale as $\mathcal{O}(N^{-2})$. Given the boundedness assumptions on r and its gradients, the moments of G_i and W_i are finite. Thus, we obtain the bound:

$$\text{Var} \left(\hat{b}_t^{(N)}(x) \right) = \sigma_t^4 \text{Var} \left(\frac{\bar{G}}{\bar{W}} \right) \leq \frac{C'}{N}. \quad (106)$$

□

We return to our main proof. We use the notation \lesssim to denote inequality up to a multiplicative constant independent of N and K , simplifying the presentation by suppressing non-essential factors.

Wasserstein-2 Bound. We use a synchronous coupling where both processes are driven by the same Brownian motion B_t . Let $e_t = \hat{X}_t - X_t^*$. The error evolves according to:

$$\frac{d}{dt} e_t = \hat{b}_{\eta(t)}^{(N)}(\hat{X}_{\eta(t)}) - b_t^*(X_t^*). \quad (107)$$

We decompose the drift mismatch as follows:

$$\hat{b}_{\eta(t)}^{(N)}(\hat{X}_{\eta(t)}) - b_t^*(X_t^*) = \underbrace{[\hat{b}_{\eta(t)}^{(N)}(\hat{X}_{\eta(t)}) - \bar{b}_{\eta(t)}(\hat{X}_{\eta(t)})]}_{\xi_t} + \underbrace{[\bar{b}_{\eta(t)}(\hat{X}_{\eta(t)}) - b_{\eta(t)}^*(\hat{X}_{\eta(t)})]}_{\Delta_t} + \underbrace{[b_{\eta(t)}^*(\hat{X}_{\eta(t)}) - b_t^*(X_t^*)]}_{D_t}, \quad (108)$$

where $\bar{b}_t(x) = \mathbb{E}[\hat{b}_t^{(N)}(x)]$ denotes the expectation over the random samples $\{\epsilon^{(i)}\}_{i=1}^N$. Integrating and taking expectations yields:

$$\mathbb{E}|e_t|^2 \lesssim \mathbb{E}\left|\int_0^t \xi_s ds\right|^2 + \mathbb{E}\left|\int_0^t \Delta_s ds\right|^2 + \mathbb{E}\left|\int_0^t D_s ds\right|^2. \quad (109)$$

Next, we bound each of the three terms separately.

Martingale Term (ξ_t). Since independent samples are used for each interval $[t_k, t_{k+1})$, the integral represents a sum of martingale increments. By orthogonality:

$$\mathbb{E}\left|\int_0^t \xi_s ds\right|^2 \leq \sum_{k=0}^{K-1} \mathbb{E}\left|\int_{t_k}^{t_{k+1}} \xi_s ds\right|^2 = \sum_{k=0}^{K-1} \delta^2 \mathbb{E}|\xi_{t_k}|^2. \quad (110)$$

Using the variance bound from Proposition C.4 ($\mathbb{E}\|\xi_{t_k}\|^2 \lesssim N^{-1}$), we have:

$$\mathbb{E}\left|\int_0^t \xi_s ds\right|^2 \lesssim \sum_{k=0}^{K-1} \delta^2 \frac{1}{N} = \frac{1}{NK}. \quad (111)$$

Bias Term (Δ_t). Using Jensen's inequality and the bias bound from Proposition C.4,

$$\mathbb{E}\left\|\int_0^t \Delta_s ds\right\|^2 \leq t \int_0^t \mathbb{E}\|\Delta_s\|^2 ds \lesssim \frac{1}{N^2}. \quad (112)$$

Discretization Term (D_t). We assume b^* is L -Lipschitz in space and $1/2$ -Hölder continuous in time. Using the triangle inequality:

$$|D_s| \leq |b_{\eta(s)}^*(\hat{X}_{\eta(s)}) - b_s^*(\hat{X}_{\eta(s)})| + |b_s^*(\hat{X}_{\eta(s)}) - b_s^*(\hat{X}_s)| + |b_s^*(\hat{X}_s) - b_s^*(X_s^*)| \quad (113)$$

$$\lesssim \sqrt{|s - \eta(s)|} + |\hat{X}_{\eta(s)} - \hat{X}_s| + |e_s|. \quad (114)$$

Integrating and taking expectation implies:

$$\mathbb{E}\left|\int_0^t D_s ds\right|^2 \lesssim \int_0^t \left(\delta + \mathbb{E}|\hat{X}_{\eta(s)} - \hat{X}_s|^2 + \mathbb{E}|e_s|^2\right) ds. \quad (115)$$

To handle the term $\mathbb{E}|\hat{X}_{\eta(s)} - \hat{X}_s|^2$, recall that $\hat{X}_s - \hat{X}_{\eta(s)} = \int_{\eta(s)}^s \hat{b}_u du + \int_{\eta(s)}^s \sigma_u dB_u$. The squared expectation is dominated by the diffusion term (via Itô isometry), which scales as the interval length δ , whereas the drift term scales as δ^2 . Thus, we have the standard Euler-Maruyama bound $\mathbb{E}|\hat{X}_{\eta(s)} - \hat{X}_s|^2 \lesssim \delta$. Substituting this back:

$$\mathbb{E}\left|\int_0^t D_s ds\right|^2 \lesssim \delta + \int_0^t \mathbb{E}|e_s|^2 ds. \quad (116)$$

Completing the Bound. Combining the terms leads to:

$$\mathbb{E}|e_t|^2 \lesssim \frac{1}{NK} + \frac{1}{N^2} + \frac{1}{K} + \int_0^t \mathbb{E}|e_s|^2 ds. \quad (117)$$

Applying Grönwall's lemma:

$$\sup_{t \in [0,1]} \mathbb{E}|e_t|^2 \lesssim \frac{1}{NK} + \frac{1}{N^2} + \frac{1}{K}. \quad (118)$$

Taking square root and only keeping the dominant terms yields the Wasserstein-2 bound:

$$W_2(\hat{p}_1, p_{\text{reward}}) \leq \sqrt{\mathbb{E}|e_1|^2} \lesssim \frac{1}{\sqrt{K}} + \frac{1}{N}. \quad (119)$$

KL Divergence Bound. We employ the data-processing inequality to bound the divergence between the sampling distribution and the target by the divergence between their path measures: $\text{KL}(\hat{p}_1 \| p_{\text{reward}}) \leq \text{KL}(\mathbb{P}^{\hat{X}} \| \mathbb{P}^{X^*})$. The process \hat{X} follows $d\hat{X}_t = \hat{b}_{\eta(t)}^{(N)}(\hat{X}_{\eta(t)})dt + \sigma_t dB_t$, while the optimal target process X^* follows $dX_t^* = b_t^*(X_t^*)dt + \sigma_t dB_t$. Let \mathcal{G}_t denote the filtration generated by the Brownian motion up to time t and the sequence of independent random samples used to construct the drift estimators at steps $t_k \leq t$. Under the boundedness assumptions, Novikov's condition holds and Girsanov's theorem applies, so the KL divergence is given by:

$$\text{KL}(\mathbb{P}^{\hat{X}} \| \mathbb{P}^{X^*}) = \frac{1}{2} \int_0^1 \mathbb{E} \left[\sigma_t^{-2} \left| \hat{b}_{\eta(t)}^{(N)}(\hat{X}_{\eta(t)}) - b_t^*(\hat{X}_t) \right|^2 \right] dt. \quad (120)$$

Assuming $\sigma_t \geq \sigma_{\min} > 0$, we can bound the integrand by the Mean Squared Error (MSE) of the drift. We decompose the error at time t into the same three components ξ_t , Δ_t , and D_t used in the Wasserstein analysis and obtain:

$$\text{KL}(\mathbb{P}^{\hat{X}} \| \mathbb{P}^{X^*}) \lesssim \int_0^1 (\mathbb{E}|\xi_t|^2 + \mathbb{E}|\Delta_t|^2 + \mathbb{E}|D_t|^2) dt. \quad (121)$$

We now bound the integrated MSE of each term. Crucially, notice that we must bound the integral of the expectations, which differs from the expectation of the squared integral in the Wasserstein analysis (109).

Variance Term ($\mathbb{E}|\xi_t|^2$). This term represents the variance of the gradient estimator. By Proposition C.4, $\mathbb{E}|\xi_t|^2 \lesssim N^{-1}$. Thus:

$$\int_0^1 \mathbb{E}|\xi_t|^2 dt \lesssim \frac{1}{N}. \quad (122)$$

Bias Squared Term ($\mathbb{E}|\Delta_t|^2$). By Proposition C.4, the bias satisfies $\|\Delta_t\| \lesssim N^{-1}$. Consequently, the squared bias scales quadratically:

$$\int_0^1 \mathbb{E}|\Delta_t|^2 dt \lesssim \frac{1}{N^2}. \quad (123)$$

Discretization Term ($\mathbb{E}|D_t|^2$). Recall that the discretization error is defined as $D_t = b_{\eta(t)}^*(\hat{X}_{\eta(t)}) - b_t^*(\hat{X}_t)$. Using the L -Lipschitz spatial condition and 1/2-Hölder time condition on b^* :

$$|D_t| \leq |b_{\eta(t)}^*(\hat{X}_{\eta(t)}) - b_t^*(\hat{X}_{\eta(t)})| + |b_t^*(\hat{X}_{\eta(t)}) - b_t^*(\hat{X}_t)| \lesssim \sqrt{|t - \eta(t)|} + |\hat{X}_{\eta(t)} - \hat{X}_t|. \quad (124)$$

Squaring and taking expectations, we apply the standard Euler-Maruyama estimate $\mathbb{E}|\hat{X}_{\eta(t)} - \hat{X}_t|^2 \lesssim \delta$. Since $|t - \eta(t)| \leq \delta$, we obtain the pointwise bound $\mathbb{E}|D_t|^2 \lesssim \delta$. Integrating over $[0, 1]$ yields:

$$\int_0^1 \mathbb{E}|D_t|^2 dt \lesssim \delta = \frac{1}{K}. \quad (125)$$

Completing the Bound. Summing the contributions and keeping dominant terms yields:

$$\text{KL}(\hat{p}_1 \| p_{\text{reward}}) \lesssim \frac{1}{N} + \frac{1}{K}. \quad (126)$$

□

D GLASS Flows (Holderrieth et al., 2025)

In this section, we provide additional background on GLASS Flows (Holderrieth et al., 2025). GLASS Flows provides the methodology for sampling from the conditional posterior $p_{1|t}(\cdot|x)$ of a Gaussian probability path using an ODE. The core insight is that when the prior p_0 is Gaussian, the drift, \bar{b}_s , targetting this conditional posterior can be derived by a re-parametrization of the denoiser D_t , and hence, the drift $b_t(x)$:

$$\bar{b}_s(\bar{x}_s; t, x) = w_1(s)\bar{x}_s + w_2(s)D_{t^*}(S(\bar{x}_s, x)) + w_3(s)x \quad (127)$$

where $w_1(s) = \frac{\dot{\alpha}_s}{\alpha_s}$, $w_2(s) = \dot{\beta}_s - \beta_s w_1(s)$, $w'_3(s) = -\bar{\gamma} w_1(s)$ are scalar coefficients, t^* is a re-parametrized time, S is a linear sufficient statistic, and $\bar{\gamma} = \rho\alpha_s\alpha_t$ with $1 \leq \rho \leq 1$ denoting a free parameter (the correlation between x_s and x in their joint distribution conditioned on data). We can re-write this re-parametrization in terms of the unconditional drift $b_t(x)$, instead of the denoiser $D_t(x)$, as the two are related as follows:

$$D_{t^*}(S(\bar{x}_s, x)) = \frac{b_{t^*}(S(\bar{x}_s, x)) - \frac{\dot{\alpha}_s}{\alpha_s} S(\bar{x}_s, x)}{\dot{\beta}_s - \frac{\dot{\alpha}_s}{\alpha_s} \beta_s} \quad (128)$$

We further map the notations and variables in Holderrieth et al. (2025) to the notation used in our presentation of MFM in Table 3.

Concept	GLASS (Holderrieth et al., 2025)	MFM (Ours)
Clean Data	$z \sim p_{\text{data}}$	$x_1 \sim p_1$
Noise	$\epsilon \sim \mathcal{N}(0, I)$	$x_0 \sim p_0$
Interpolant	$x_t = \alpha_t z + \sigma_t \epsilon$	$I_t = \beta_t x_1 + \alpha_t x_0$
Unconditional Drift	$u_t(x)$	$b_t(x)$
Denoiser	$D_t(x) = \mathbb{E}[z x_t = x]$	$D_t(x) = \mathbb{E}[x_1 I_t = x]$

Table 3 Translation of notation between GLASS Flows and MFM.

E Algorithms

Algorithm 4 One-step MFM Sampler

Require: MFM X .

- 1: Sample $\epsilon \sim p_0$
 - 2: $\hat{x}_1 \leftarrow X_{0,1}(\epsilon; 0, \vec{0})$.
 - 3: **return** \hat{x}_1
-

Algorithm 5 K -Step $\gamma = 1$ -Sampler

Require: MFM X , times $0 = t_0 < \dots < t_K = 1$.

- 1: Sample $x_0 \sim p_0$
- 2: **for** $k = 0, \dots, K - 1$ **do**
- 3: $x_0^{(k)} \sim p_0$
- 4: $\hat{x}_1^{(k)} \leftarrow X_{t_k, 1}(x_{t_k}; 0, \vec{0})$
- 5: $x_{t_{k+1}} \leftarrow \alpha_{t_{k+1}} x_0^{(k)} + \beta_{t_{k+1}} \hat{x}_1^{(k)}$
- 6: **end for**
- 7: **return** x_1

Algorithm 6 MFM Steering (SDE)

Require: Reward $r(x)$; MFM X ; times $0 = t_0 < \dots < t_K = 1$; MC batch size N .

- 1: Initialize $X_0 \sim p_0$
- 2: **for** $k = 0, \dots, K - 1$ **do**
- 3: $dt \leftarrow t_{k+1} - t_k$
- 4: $\sigma_{t_k}^2 \leftarrow 2(\frac{\dot{\beta}_{t_k}}{\beta_{t_k}} \alpha_{t_k}^2 - \dot{\alpha}_{t_k} \alpha_{t_k})$
- 5: $b_{t_k}(X_{t_k}) \leftarrow v_{t_k, t_k}(X_{t_k}; 0, \vec{0})$ as in (36)
- 6: Extract $\nabla \log p_{t_k}(X_{t_k})$ by a reparametrization
- 7: Sample iid $\epsilon^{(n)} \sim p_0$ for $n = 1, \dots, N$
- 8: $\hat{x}_1^{(n)} \leftarrow X_{0, 1}(\epsilon^{(n)}, t_k, X_{t_k})$
- 9: Estimate $\widehat{V_{t_k}(X_{t_k})} \leftarrow \log\left(\frac{1}{N} \sum_{n=1}^N e^{r(\hat{x}_1^{(n)})}\right)$
- 10: Compute $\nabla \widehat{V_{t_k}(X_{t_k})} \leftarrow \nabla_{X_{t_k}} \log\left(\frac{1}{N} \sum_{n=1}^N e^{r(\hat{x}_1^{(n)})}\right)$ via (20) (or alternatively can use (22))
- 11: Sample $Z \sim \mathcal{N}(0, I)$
- 12: $X_{t_{k+1}} \leftarrow X_{t_k} + dt \left(b_{t_k}(X_{t_k}) + \frac{\sigma_{t_k}^2}{2} \nabla \log p_{t_k}(X_{t_k}) + \sigma_{t_k}^2 \nabla \widehat{V_{t_k}(X_{t_k})} \right) + \sqrt{dt} \sigma_{t_k} Z$
- 13: **end for**
- 14: **return** X_1

F Experiment Details & Additional Results

We present below additional results, extended descriptions of our experimental settings, and hyper-parameters from the experiments in our main body.

F.1 Gaussian Mixture Model

To analytically evaluate our proposed methods, we first consider a synthetic 2D problem. Specifically, we consider a 2D Gaussian mixture model with 3 components as a prior distribution p_1 , i.e. $p_1(x) = \sum_{i=1}^3 \frac{1}{3} \mathcal{N}(x; \mu_i, \Sigma_i)$, where $\mu_1 = (-3, -3)$; $\mu_2 = (0, 0)$; $\mu_3 = (3, 3)$; $\Sigma_1 = \Sigma_2 = \Sigma_3 = 0.5 I_{2 \times 2}$. We train a MFM using a small MLP using the semigroup MFM loss (see 4.3). For the ODE and SDE, we use the Euler and Euler-Maruyama respectively, both with $N = 1000$ discretisation steps, for all methods presented.

For defining the inverse problem, we take the forward model as a linear measurement, $y = \mathbf{a}^T \mathbf{x} + \epsilon$, with $\mathbf{a} = [1.2, -0.8]^T$; $\epsilon \sim N(0, \sigma^2)$; $\sigma = 0.2$, and target the posterior $p(x|y = -1.0)$ under this measurement model. For evaluation, we (1) generate 4096 posterior samples, and (2) sample-to-sample metrics with samples from the true analytic posterior.

F.2 MNIST

For MNIST, we train a 9M parameter UNet-based MFM using the semigroup MFM loss (see 4.3). For defining the reward model, we use a simple CNN-based classifier. As with GMMs, we use Euler and Euler-Maruyama

samplers, but with $N = 500$ discretisation steps, for all methods presented. For defining the reward, we take $\mathbf{w} = [0, 1, 0, 1, 0, 2, 0, 2, 0, 4]$ which defines a highly multimodal, imbalanced target distribution.

F.3 ImageNet (256 × 256)

For ImageNet (256 × 256), we train MFM by adapting DiT architectures, at B/2 and XL/2 scale, to allow for conditioning on (t, x) (See B.2 for further details). These adaptations result in a small relative increase in the number of parameters, 131 → 134M and 675 → 684M respectively.

MFM B/2. We train a B/2 model using data. We initialise the model with the weights of a well-trained flow model, SiT B/2. As the unconditional instantaneous velocity is well learned at the start of training, the focus is on 1) learning to condition on (t, x) , and 2) self-distillation into a flow-map.

MFM XL/2. We train XL/2 models using both data, and distillation. For both variants, we initialise at a well-trained flow-map checkpoint, DMF XL/2+ (Lee et al., 2025), for faster convergence. For the distillation variants, we regress onto the conditional drift extracted from a copy of DMF XL/2+ using GLASS Flows (see Equation 32).

For training from data, we leverage the Mean Flow MFM objective, and for distillation, we leverage Eulerian (Teacher) objective (See Table 1). This design choice was made to align with the standard flow-map objective used for training DMF XL/2+, the model used for initialisation. We leave a comprehensive benchmarking of the design space to future work.

F.3.1 FID

In Table 4, we present few-step FIDs of several configurations, including different model scales and objectives. In general, we took $(p_{diag} = 1.0, p_{cons} = 1.0)$ as the adaptive loss coefficients (See Equation 66) following Mean Flow (Geng et al., 2025a). However, we found that $(p_{diag} = 0.5, p_{cons} = 1.0)$ was marginally more performant configuration for 2 and 4-step generation in our XL/2 experiments.

Table 4 FID scores for increasing NFE and model scales. Lower is better. Numbers in the brackets indicate the p parameter of adaptive loss for diagonal and consistency terms of the loss function, respectively. Note that c parameter is fixed to be 0.01. See Table 5 for further configuration details of MFM.

Model	NFE			
	1	2	4	8
B/2				
Data (1.0, 1.0)	8.71	6.84	6.57	6.55
XL/2				
Data (1.0, 1.0)	4.18	4.18	4.14	4.41
Distill (1.0, 1.0)	3.65	2.70	2.17	2.18
Distill (0.5, 1.0)	3.72	2.40	1.97	2.45

F.3.2 Number of Function Evaluations (NFEs)

MFM-GF. For a K -step discretisation of the continuous-time ODE, with N posterior samples for drift estimation at each step, MFM-GF requires

$$\text{NFE} = K + 2NK.$$

This consists of K evaluations of the base drift, and at each step N one-step posterior samples and N reward evaluations to estimate the value function.

Table 5 Configurations for ImageNet experiments.

	MFM-B/2	MFM-XL/2+
<i>Model</i>		
Resolution	256×256	256×256
Params (M)	134	683
Hidden dim.	768	1152
Heads	12	16
Patch size	2×2	2×2
Sequence length	256	256
Layers	12	28
Encoder depth	8	20
<i>Optimization</i>		
Optimizer	AdamW (Kingma et al., 2017)	
Batch size	256	
Learning rate	1e-4	
Adam (β_1, β_2)	(0.9, 0.95)	
Adam ϵ	1e-8	
Adam weight decay	0.0	
EMA decay rate	0.9999	
<i>Flow model training</i>		
Training iteration	800K	4M
Epochs	160	800
Class dropout probability	0.2	0.2
Time proposal μ_{FM}	0.0	-
REPA alignment depth	-	8
REPA vision encoder	-	DINOv2-B/14
QK-norm	✗	✗
<i>DMF flow map training</i>		
Training iteration	-	400K
Epochs	-	80
Class dropout probability	-	0.1
Time proposal μ_{FM}	-	0.0
Time proposal ($\mu_{\text{MF}}^{(1)}, \mu_{\text{MF}}^{(2)}$)	-	(0.4, -1.2)
Model guidance scale ω	-	0.6
Guidance interval	-	[0.0, 0.7]
<i>MFM training</i>		
Training iteration	100K	100K
Batch size	512	360
Epochs	40	28
Optimizer	RAAdam (Liu et al., 2021)	
Learning rate	1e-4	
Learning rate warmup	Linear (first 2000 steps)	
RAAdam (β_1, β_2)	(0.9, 0.999)	
RAAdam ϵ	1e-8	
RAAdam weight decay	0.0	
EMA decay rate	0.9999	
Class dropout probability	0.2	
Model guidance scale ω	0.6	
Guidance interval	[0.0, 1.0]	

MFM-G. For a K -step discretisation of the continuous-time ODE, with N posterior samples for drift estimation at each step, MFM-G requires

$$\text{NFE} = K + 4NK.$$

This includes K base drift evaluations and, at each step, N one-step posterior samples and N reward evaluations for value estimation. MFM-G additionally requires a backward pass through the $2N$ network evaluations at each step; which we assume to incur a $2\times$ multiplicative cost.

Best-of- N baseline. Using N_{BoN} samples, the Best-of- N baseline requires

$$\text{NFE} = KN_{\text{BoN}} + N_{\text{BoN}}.$$

This corresponds to generating N_{BoN} samples using K discretisation steps, followed by a final reward evaluation for each sample required for selecting the highest-reward sample.

F.3.3 Additional Steering Results

Below, we present additional results on steering using the MFM-G and MFM-GF estimators. Here, we evaluate the reward of generations using **other** image rewards to the one used for steering. This is a crucial check, as it is important that improved rewards under the model used for steering does not stem from *reward-hacking*, which would worsen other related metrics. The performance of the model used for steering is presented in the first, emboldened subplot, with other metrics presented to the right.

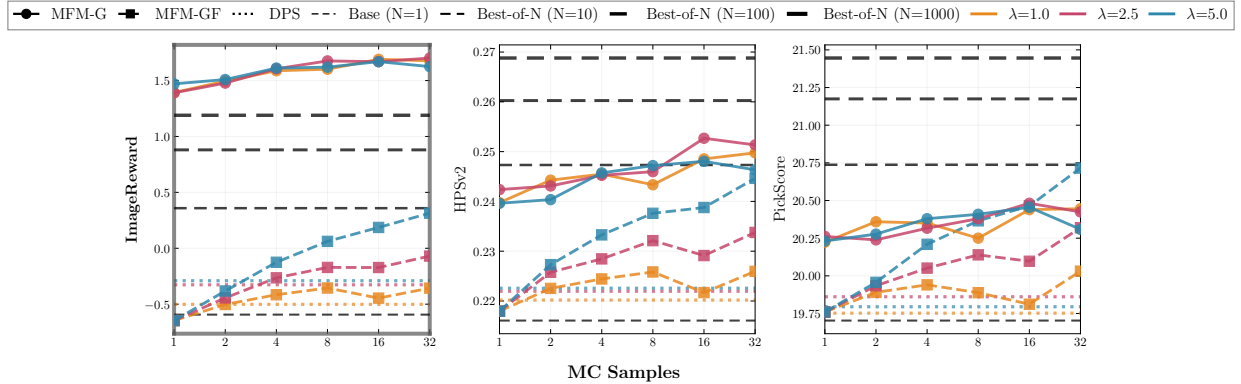


Figure 12 Metrics for steering using *ImageReward*

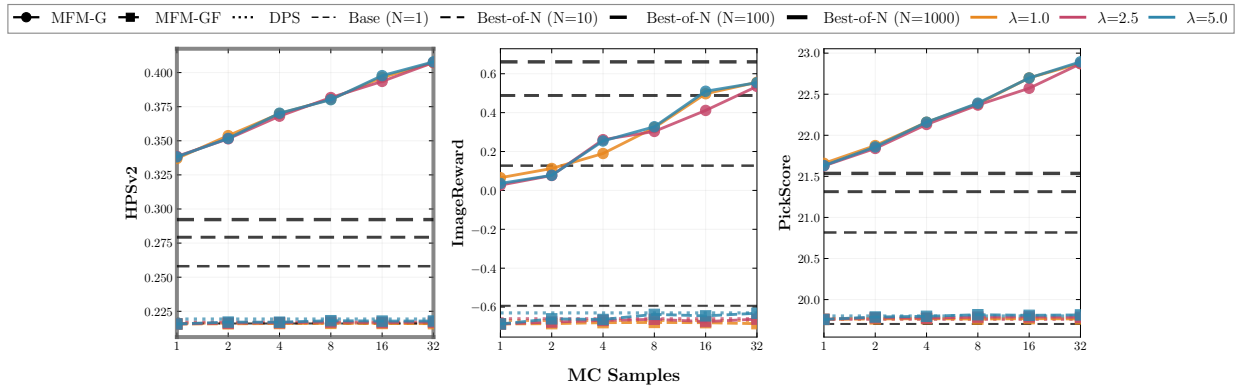


Figure 13 Metrics for steering using *HPSv2*

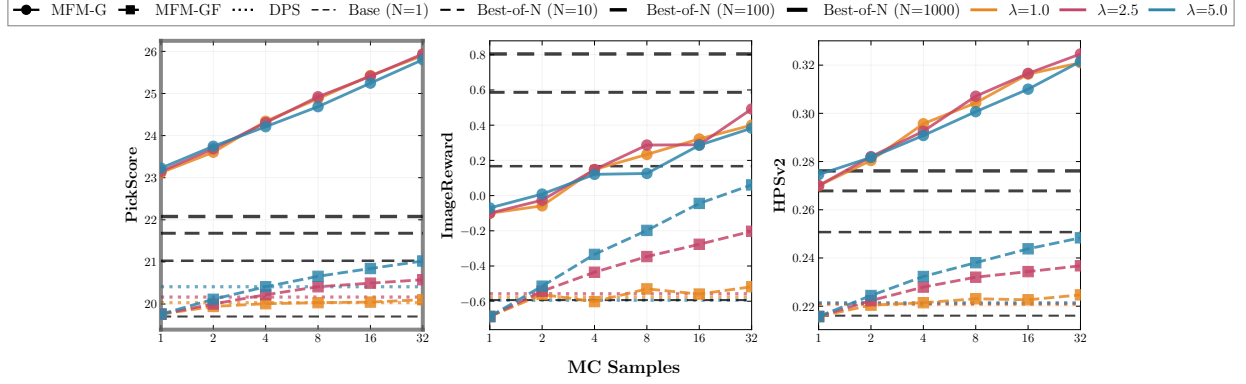


Figure 14 Metrics for steering using *PickScore*

F.3.4 Normalisation of Steered Drift Estimator

In ImageNet experiments, we encountered steering drifts much larger in magnitude than the unconditional drift. In order to faithfully realise the steered dynamics in such settings, we would require a much finer time discretisation than is required for unconditional generation to avoid excessive discretisation error. For practical implementation, we considered two different solutions, 1) *clipping* and 2) *rescaling* the steering drift relative to the norm of the unconditional drift. Although this introduces a bias, it is only in the magnitude of the drift and not the direction. As it was both highly stable and performant, we used the *rescaling* in all our ImageNet inference-time steering experiments, with $\lambda = 1$:

$$b_t^*(x) = b_t(x) + \lambda \|b_t(x)\|_2 \frac{\nabla V(x)}{\|\nabla V(x)\|_2}. \quad (129)$$

F.3.5 Additional Steered Generations

Below, we present a larger set of generations from the Base MFM and from using MFM-G for steering (HPSv2 reward model), for $\{1, 8, 16, 32\}$ samples in the MC estimate.



Figure 15 Base MFM Generations



Figure 16 MFM-G ($N = 1$)



Figure 17 MFM-G ($N = 8$)



Figure 18 MFM-G ($N = 16$)



Figure 19 MFM-G ($N = 32$)

F.3.6 Additional Fine-tuned Generations

Below, we present a larger set of generations using the base and fine-tuned MFMs ($\lambda = \{10, 25, 50\}$).



Figure 20 Base MFM

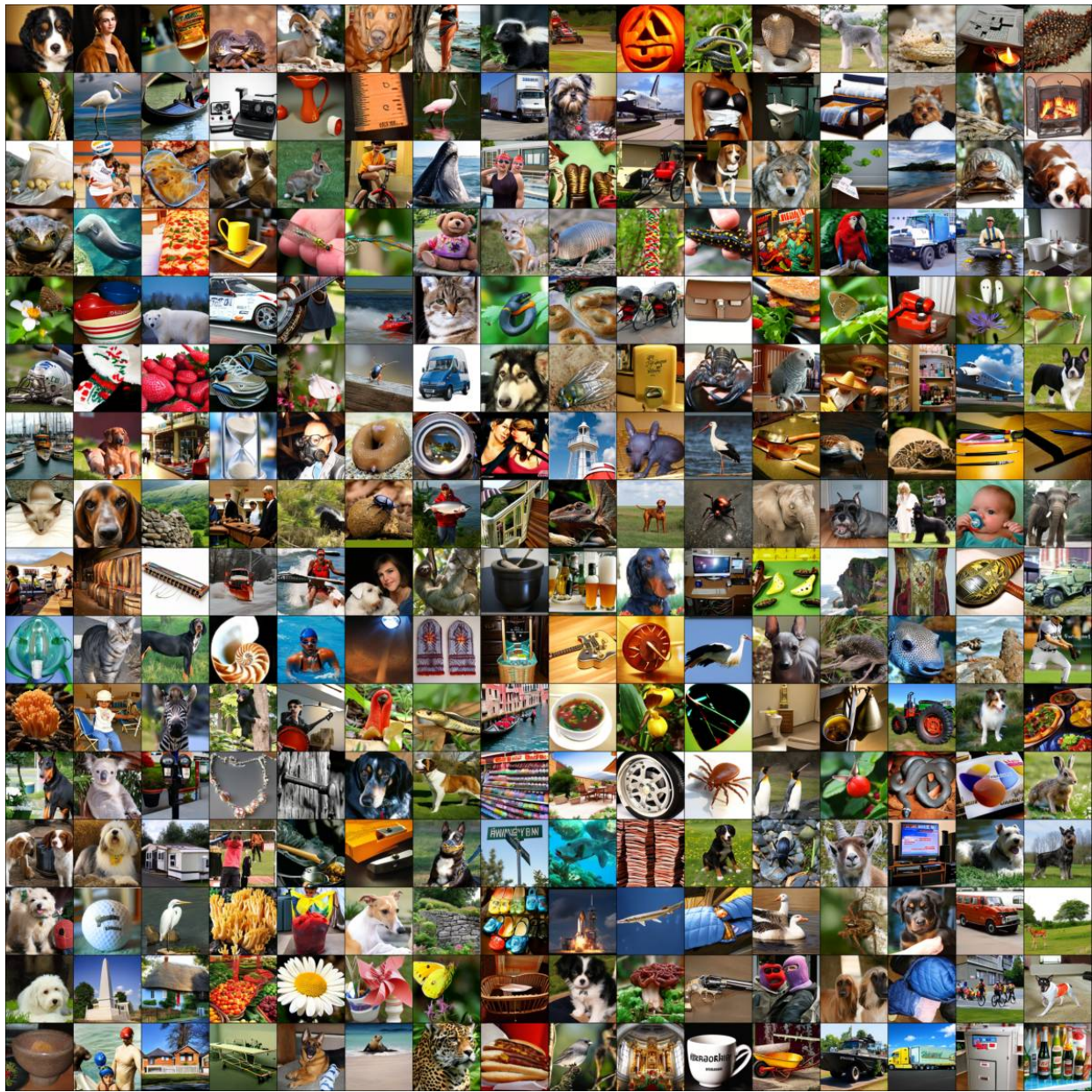


Figure 21 MFM-Finetuned ($\lambda = 10$)



Figure 22 MFM-Finetuned ($\lambda = 25$)



Figure 23 MFM-Finetuned ($\lambda = 50$)